Plant Stress 18 (2025) 101051

Contents lists available at ScienceDirect

Plant Stress

journal homepage: www.sciencedirect.com/journal/plant-stress

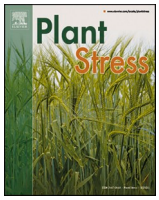

Deciphering heat-enhanced resistance of grapevine berries to *Botrytis cinerea* highlights differential cuticular and secondary metabolite accumulations between Merlot and Cabernet Sauvignon

Erwan Chavonet [a], Cathleen Mirande-Ney [b], Sarah Bernardo [a], Clément Guinand [a], Ghislain Delestre [c], Xi Zhan [d], Josep Valls Fonayet [e,f], Sylvain Prigent [b,f], Pierre Van Delft [a,f], Stéphanie Pascal [a], Jérôme Joubès [a], David Lecourieux [d,*], Marc Fermaud [c,*], Frédéric Domergue [a,*]

[a] Univ. Bordeaux, CNRS, LBM, UMR 5200, F-33140 Villenave d'Ornon, France
[b] Univ. Bordeaux, INRAE, BFP, UMR 132, F-33140 Villenave d'Ornon, France
[c] INRAE, Bordeaux Sciences Agro, ISVV, SAVE, UMR 1065, F-33882 Villenave d'Ornon, France
[d] Univ. Bordeaux, Bordeaux Sciences Agro, INRAE, ISVV, EGFV, UMR 1287, F-33882 Villenave d'Ornon, France
[e] Univ. Bordeaux, Bordeaux INP, INRAE, OENO, UMR 1366, ISVV, F-33140 Villenave d'Ornon, France
[f] Bordeaux Metabolome, MetaboHUB, F-33140 Villenave-d'Ornon, France

ARTICLE INFO

Keywords:
Gray mold
Heat stress
Ripening
Cuticle
Tannins
Stilbenes
Metabolomics

ABSTRACT

In the context of climate change, temperature is a key abiotic driver of bunch microclimate, which, in order to reduce *Botrytis cinerea* development, is often managed in vineyards *via* practices such as leaf removal. The heat-dependent mechanisms of pathogen resistance in grapevines nevertheless remain to be fully elucidated. In this study, the effect of heat stress (HS) applied specifically to green bunches on infections caused by *B. cinerea* on ripe berries inoculated 23 days later was assessed for two years in a greenhouse. Bunches of the Cabernet Sauvignon (CS) and Merlot (M) cultivars were heated 6 days 8 h daily with a 10 °C increased temperature. *In vitro* bio tests highlighted a significant heat-enhanced resistance only in CS berries, whereas a stable constitutive resistance characterized the M berries. Bunch veraison and total sugar content were not affected by HS, rejecting its effect on maturation dynamics. Therefore, berry preformed barriers at the time of inoculation, which can hinder fungal colonization, were investigated. While HS had nearly no effect on waxes, it significantly affected the cutin content in both varieties, and more significantly its composition in CS. Similarly, the antifungal skin condensed tannins overaccumulated following HS in both cultivars, and their basal level was greater in CS than in M. Otherwise, M accumulated more stilbene and flavonoid compounds, which may have contributed to the observed varietal resistance. Finally, untargeted metabolomic data revealed a range of compounds modulated by HS in CS as potential candidates involved in resistance.

Introduction

The necrotrophic cosmopolite fungus *Botrytis cinerea* is responsible for gray mold disease in grapevine (*Vitis vinifera* L.) bunches, and uncontrolled outbreaks lead to severe yield losses (Rahman et al., 2024). The onset of gray mold disease occurs on bunches after veraison (Elmer and Michailides, 2007), with symptoms subsequently increasing with fruit ripening (Deytieux-Belleau et al., 2009; Kretschmer et al., 2007). Early infection of floral tissues by *B. cinerea* are known as a major determinant of gray mold incidence and severity in grapevine bunches notably because the floral organs are highly susceptible and can serve as entry points for quiescent infections (Elmer and Michailides, 2007; Viret et al., 2004). Furthermore, the efficacy of fungicidal and/or biological treatments applied during full-bloom highlights the importance of this early stage (Calvo-Garrido et al., 2014; Fedele et al., 2020; Wang et al., 2023). Alternatively, infection may also accur directly by conidia or hyphae deposition on the fruit surface after veraison stage (Elmer and Michailides, 2007). Once the skin has been crossed, the underlying

* Corresponding authors.
E-mail addresses: david.lecourieux@u-bordeaux.fr (D. Lecourieux), marc.fermaud@inrae.fr (M. Fermaud), frederic.domergue@u-bordeaux.fr (F. Domergue).

https://doi.org/10.1016/j.stress.2025.101051
Received 28 May 2025; Received in revised form 8 September 2025; Accepted 23 September 2025
Available online 24 September 2025

tissues necrotize as the fungus progresses through the berries, and mycelial and sporulating structures gradually cover the berry surface (Kelloniemi et al., 2015; Rahman et al., 2024; Weiller et al., 2021). Subsequently, the contamination of large portions of whole bunches usually occurs through contacts between infected and healthy berries, and thus the effect of *B. cinerea* is highly dependent on bunch compactness (Hed et al., 2009; Molitor et al., 2012). In compact bunches, the spread of *B. cinerea* may be promoted by several factors, including (i) elevated humidity and/or wetness within the cluster due to restricted ventilation and limited sun exposure; (ii) increased risk of berry splitting due to pressure between berries (iii) berry-to-berry fungal transmission; and (iv) thinner cuticle layers at contact points promoting pathogen penetration (Molitor et al., 2012). Furthermore, a limited fungicide penetration inside the bunch or a greater accumulation of dehiscent floral debris that are potential inoculum source, are considered as complementary factors (Hed et al., 2009).

Preformed physical and chemical barriers of berries contribute to preventing infection by *B. cinerea* (Rahman et al., 2024). Indeed several skin features such as cuticle structure or cell wall composition determine the initial penetration step (André et al., 2021; Comménil et al., 1997; Deytieux-Belleau et al., 2009; Gabler et al., 2003; Herzog et al., 2022; Kretschmer et al., 2007). In addition, the presence of natural openings or lesions allows the fungus to bypass the skin barrier, which accelerates fungal colonization (Kretschmer et al., 2007). Otherwise, *B. cinerea* early deploys specialized hyphal structures known as unicellular appressoria or multicellular infection cushions to mediate surface adhesion and tissue penetration. These structures generate through osmolyte accumulation a high turgor pressure (27–42 bar), enabling an actin-dependent penetration peg to breach the host cuticle and cell wall (Müller et al., 2024). Simultaneously, these infection structures secrete lytic enzymes—including cutinases, cellulases, and lipases—which facilitate the breakdown of cuticle and cell wall polymers, suggesting that tissue invasion results from the synergistic action of mechanical force and localized enzymatic degradation (Choquer et al., 2021; Kelloniemi et al., 2015).

The berry cuticle is the first barrier *B. cinerea* encounters (Choquer et al., 2021; Comménil et al., 1999, 1997). Although similar cuticular components are generally found in different varieties and developmental stages, their contents, as well as the berry cuticle thickness and morphology, can differ (Arand et al., 2021; Pensec et al., 2014; Radler, 1965; Zhang et al., 2021). The plant cuticle is a lipophilic barrier subdivided into two compartments: (i) an external layer of wax deposited onto and interlocked with (ii) a deeper cutin layer, which is integrated into the cell wall to a certain extent (Fernández et al., 2016). Grapevine berry waxes are dominated by triterpenoid compounds, especially oleanolic acid, but also contain very long-chain fatty acids, *i.e.,* C24 to C28 acyl chains, and their primary alcohol and aldehyde derivatives (Arand et al., 2021; Pensec et al., 2014; Radler, 1965; Zhang et al., 2021). The majority of monomers making the cutin polyester are C18 polyhydroxylated and epoxylated fatty acids (Boulet et al., 2025). After veraison, the cuticle amount per surface area decreases (Arand et al., 2021; Comménil et al., 1997; Zhang et al., 2021), in line with a thickness reduction, both of which are correlated with the predisposition of the berries to become more infected as ripening progresses (Comménil et al., 1997).

After crossing the cuticular barrier, the fungus quickly triggers cell wall breakdown by secreting a cocktail of degrading enzymes targeting cellulose, hemicellulose and pectin (Blanco-Ulate et al., 2014; Kelloniemi et al., 2015; Weiller et al., 2021). Cell wall hydrolysis allows *B. cinerea* to gain access to cells and to use the resulting degradation products as nutrient sources (Blanco-Ulate et al., 2016). Hence, berry skin cell wall thickness and polysaccharide composition act as additional physical barriers hindering fungus progression, and are therefore associated with varietal resistance against *B. cinerea* (André et al., 2021; Weiller et al., 2021).

Stilbenic phytoalexins constitute an additional layer of defense that is induced when berries are challenged by pathogenic fungi (Viret et al., 2018). Fungitoxic stilbenes, such as resveratrol, have been shown to inhibit the germination and growth of *B. cinerea in vitro* (Adrian et al., 1997; Xu et al., 2018), and its overaccumulation in berries at veraison either through the salicylic acid pathway (Kelloniemi et al., 2015) or by benzothiadiazole elicitation (Iriti et al., 2004) has been shown to improve resistance. Conversely, the ability of *B. cinerea* to detoxify stilbenes is essential for its pathogenicity (Adrian et al., 1998; Pezet et al., 1991; Sbaghi et al., 1996), and a gradual decrease in the levels of these phytoalexins a few days after the peak triggered by infection has been reported (Montero et al., 2003). However, the presence of flavonoids and other phenolics in berries can inhibit stilbene oxidase, which hinders the ability of the fungus to fully and rapidly degrade stilbenic defenses (Goetz et al., 1999; Perret et al., 2003).

In the wine-making cultivars, the berry skin is also enriched in oenological tannins including hydrolysable tannins (gallotannins and ellagitannins) and condensed tannins (or proanthocyanidins). The condensed tannins correspond to oligomers or polymers of flavan-3-ol and are in part deposited inside the cell wall of berry skins (Gagné et al., 2006; Lecas and Brillouet, 1994; Watrelot and Norton, 2020). Both hydrolysable—notably gallotannins—and condensed tannins from the grape skin were shown to prevent damage by key degrading enzymes from *B. cinerea, i.e.* by reducing significantly laccase activity (Vignault et al., 2020; 2019). Specifically, tannins were shown to protect stilbenes from degradation by *B. cinerea* stilbene oxidase (Goetz et al., 1999), and to inhibit *B. cinerea* pectinases that target the cell wall (Porter and Schwartz, 1962; Scalbert, 1991). Furthermore, proanthocyanidins were suggested to keep *B. cinerea* in a quiescent state (van Baarlen et al., 2007). Since condensed tannins have been highly correlated with a decreased final disease severity in vineyards, their quantification was proposed as a possible early predictor of berry susceptibility (Deytieux-Belleau et al., 2009; Paňitrur-De La Fuente et al., 2020).

As highlighted by the conceptual model of the disease triangle, the infection outcome not only results from the host–pathogen relationship but also depends on environmental parameters (Scholthof, 2007). It is well known that gray mold epidemiology is driven by weather conditions and that its spread in vineyards, for example, is favored by cumulative rainfall (Evans and Pirie, 2024). By extension, microclimate features such as temperature, wind speed, wetness and relative humidity influence fungal incidence and severity (Broome et al., 1995; Thomas et al., 1988). Leaf removal at the bunch level is a common viticultural practice that reduce the wetness and relative humidity of berries to manage *B. cinerea* occurrence (Hed and Centinari, 2024; Molitor et al., 2011; Würz et al., 2020). Unfortunately, the responses of grapevines to such abiotic changes possibly responsible for increased *B. cinerea* resistance remain largely understudied. An increase in pellicular antifungal compounds, corresponding to condensed tannins in Merlot (Paňitrur-De La Fuente et al., 2020) and specifically eugenol in Baco blanc (Hastoy et al., 2023), was shown to be associated with improved resistance against *B. cinerea*. Importantly, leaf removal modifies not only the humidity surrounding the berries but also the temperature, which usually increases because of bunch solar exposure, possibly causing heat stress (HS; Sternad Lemut et al., 2013). Although grapevine varietal responsiveness to HS has been extensively studied (Carvalho et al., 2015; Hewitt et al., 2023; Wu et al., 2023; Xu et al., 2014), it is less clear whether the host response to a pathogen following HS is also dependent on the host's genetic background. In addition, the interactions of HS with pathogen susceptibility and subsequent disease development still need to be further explored. A better understanding of varietal responses to multiple stresses, notably involving HS and pathogens, would be particularly useful to better anticipate the environmental impact on vineyard health with regards to the planted cultivars (Shelake et al., 2024), especially in the context of current climate change.

A heat increase applied exclusively to bunches was previously shown to reprogram the transcriptome, proteome and metabolome of Cabernet Sauvignon (CS) berries (Lecourieux et al., 2020, 2017). Although HS has

a detrimental effect on proteins and secondary metabolism, such as flavonoid biosynthesis, several mechanisms are triggered in response to this abiotic stress. These include the accumulation of protein chaperones and protective metabolites, including antioxidants, and the mobilization of enzymes possibly involved in reinforcing constitutive barriers such as lignin and cuticle. Therefore, HS may affect several key metabolites that are potential determinants of the interaction with *B. cinerea*. In this study, we investigated the effects of HS applied for 6 days exclusively to herbaceous bunches on subsequent *B. cinerea* infection. *B. cinerea* colonization was evaluated *in vitro* on detached berries from two French wine varieties, CS and Merlot (M), more than 3 weeks after HS. We hypothesized that abiotic stress prior to conditions favorable to the disease, *i.e.,* favorable microclimate and berry maturity, can play a role in fungal pathogenesis through the modulation of preformed defenses and/or virulence-promoting factors. As we showed that berry ripening and physiology were not affected by HS, our work focused on the consequences of HS on cuticular compounds, condensed tannins in the skin and the entire berry metabolome, providing an overview of potential heat-dependent metabolites linked to resistance against *B. cinerea*.

Materials and methods

Plant material

Fruiting cuttings of *Vitis vinifera* L., cv. CS and M (Supplemental Figure 1A), were prepared as described by Ollat et al. (1998) with adjustments as follows. After root emergence (2 to 4 cm) was achieved by placing the cuttings for 4 to 6 weeks in moist vermiculite at 26 to 32 °C using heating mats while maintaining in fridge the apical buds at 4 °C (to ensure root development occurs before budburst and prevent competition for limited reserves), the plants were cultivated in a greenhouse in 0.5 L of a mixture of perlite, sand and vermiculite (1:1:1 v/v/v). Plants were irrigated with 15 to 20 mL of osmotic water per watering event 4 or 5 times/day (60–80 or 75–100 mL daily) through a drip system until the onset of blossoming. Thereafter, irrigation water was replaced with a nutrient solution, composed as described in Ollat et al. (1998), and delivered using the same system. All the leaves and apical buds of each plant were pruned to ensure that only one inflorescence fully developed, and then, 4 leaves were allowed to grow until 10–15 days after blossoming. Afterward, a single primary shoot above the bunch was allowed to grow to 1.1 m by regularly removing lateral shoots to maintain an approximately uniform leaf area between plants. This strictly controlled growth resulted in berries whose development and composition were similar to those of the berries sampled in vineyards (Dai et al., 2014; Geny et al., 1998).

Heat-exposure experimental device

In this study, similar experiments were conducted for 2 years, *i.e.,* May to July 2023 and June to August 2024 (Fig. 1A). Both the control (CTRL) and HS treatments were applied only to bunches at the end-green stage (*i.e.*, approximately 6 weeks after flowering and 10 days before the beginning of veraison for half of all the plants) in a greenhouse equipped with a cooling system. To mimic leaf removal practices,

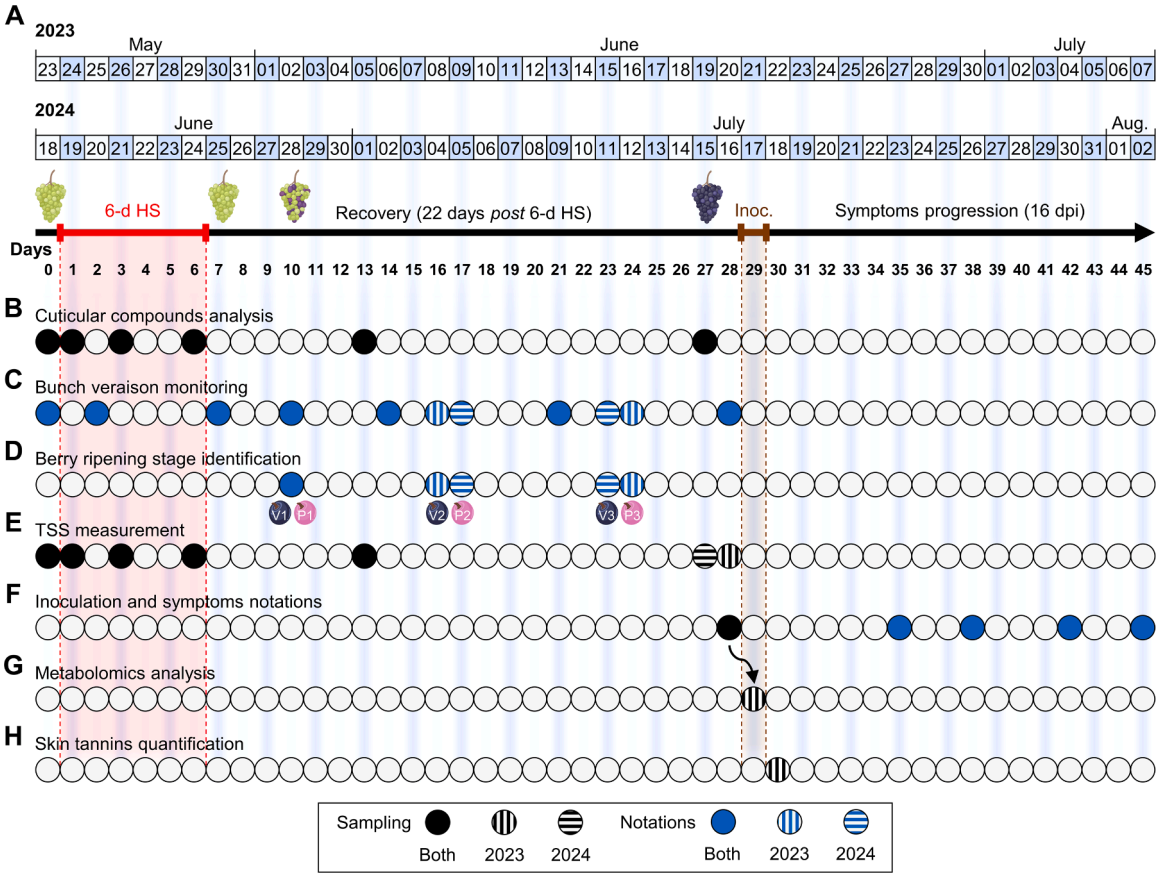

Fig. 1. Sampling and notations performed during both 2023 and 2024 trials. (A) Experimental calendars showing the periods of HS, recovery, inoculation, and symptoms annotation. (B) Sampling dates for collecting berries dedicated to cuticular compounds analysis. (C) Sampling dates for bunch veraison monitoring evaluated by the proportion of ripe berry. (D) Sampling dates for Bberries banding to determine their ripening stage. V, violet; P, pink. (E) Sampling dates for collecting berries dedicated to total soluble solids (TSS) measurement. (F) Sampling dates for collecting berries dedicated to the next day inoculation and for evaluating of symptoms 6, 9, 13 and 16 dpi. (G) Sampling date for collecting detached berries, *i.e.*, as for those inoculated, for metabolomics analysis. (F) Sampling date for collecting berries dedicated to skin condensed tannins assays in 2023. Icons created in BioRender.com.

bunches were heated by exposure to airflow produced by oscillating fan heaters (2000 W oscillating fan heaters Warm Tech and FH-726 for 2023 and 2024, respectively) set to 1000 W (Supplemental Figure 1B), while control plants were blown with ambient air (Supplemental Figure 1C). Shoots, leaves and roots from heated plants were insulated from increased temperatures with extruded polystyrene foam deflectors so that only the bunches were heat exposed. For both conditions, a total of 22 and 21 fruiting cuttings of CS, as well as 16 and 10 fruiting cuttings of M, were used in 2023 and 2024, respectively. Airflow was applied repeatedly for 6 days (6-d HS) for 8 h, from 8:00 a.m. to 4:00 pm., to follow the natural photoperiod. After the 6-d HS, the plants were maintained at 18 to 22 °C until the end of the trials.

Temperature and relative humidity control measurements

Berry flesh temperatures were measured with copper–constantan thermocouples inserted into berries facing the airflow and connected to a Campbell datalogger (CR1000, Campbell Scientific; Supplemental Figure 1D). The mean temperature was determined every 15 min from values recorded by 4 and 8 thermocouples for the CTRL and HS conditions, respectively. In both years, the flesh temperatures of 8 heated berries and 4 control berries, each from different bunches, were monitored continuously during the 6-d HS. Air temperature and relative humidity (RH) were measured in 2024 with 4 additional probes (2 for each condition; HOBO Smart Sensors, ONSET) connected to a HOBO datalogger (HOBO U30 USB Station, ONSET) associated with 2 external channel data loggers (both placed only in heated conditions, HOBO U12-013, ONSET). All air probes were installed at the bunch level to determine the temperature and RH around the fruit every 6 min (Supplemental Figure 1E). The vapor pressure deficit (VPD) at the fruit level was calculated as follows (Evans and Pirie, 2024):

$$VPD\ (\text{kPa}) = \frac{\text{ES} - E}{1000} \text{ where } ES = 610.78 \times e^{\frac{Temperature \times 17.2693882}{Temperature + 237.3}}$$

$$\text{and } E = \frac{HR \times ES}{100}$$

Cuticular compound extraction and analysis

Cuticular compounds were extracted from samples comprising 5 or 3 berries in 2023 and 2024, respectively. For all samplings, berries of similar maturity according to their visual appearance (green, pink or violet color) were randomly selected from different clusters and plants (avoiding to collect multiple berries from the same cluster whenever possible). In both years, berries were sampled the day before (day 0), during (1st, 3rd and 6th days) and after (13th and 27th days after) the 6-d HS (Fig. 1B). Four and six samples per variety × temperature × sampling time were collected in 2023 and 2024, respectively (with one exception in 2023, when six samples were taken on the 13th day). The samples collected until the 6th day and the 27th day included only green and violet berries, respectively, whereas the samples collected on the 13th day included 2 samples per color. Epicuticular waxes were extracted by immersing pooled berries (with attached pedicels) for 30 s in 8 mL of chloroform with 10 µg/berry of docosane as internal standard. The total amount of epicuticular wax was expressed per unit of fruit surface. The length and width of each berry were measured with ImageJ software (v1.53k; https://imagej.net/; Schneider et al., 2012) *via* top-down photography. Each berry was considered a prolate spheroid, and the surface area was calculated with the following formula:

$$Surface\ area\ (\text{cm}^2) = 2\pi b^2 + 2\pi ab\ \frac{\arcsin(e)}{e} \text{ where } e = \frac{\sqrt{a^2 - b^2}}{a},$$

$$a = \frac{length}{2} \text{ and } b = \frac{width}{2}$$

Following wax extraction, the exocarps were separated from the flesh and immediately dipped into 2.5 mL of hot 2-propanol for 45 min at 85 °C. Exocarps were extensively delipidated at room temperature by successive 24 h washes with chloroform/methanol 2:1 and 1:1 (v/v) on a wheel (tube rotator SB3, Stuart) rotating at 33 rpm and then dried under a fume hood for 2–3 days. The dry skins were weighed to determine the cutin content per mass unit of dry residue (DR). Cutin was depolymerized by transmethylation at 85 °C for 90 min in methanol with sulfuric acid (5 %, v/v) containing 2 µg/µg DR of heptadecanoic acid, ω-pentalactone and pentadecanol as internal standards. Two hundred microliters of acidic methanol solution was mixed vigorously with 2.2 mL of methyl *tert*-butyl ether (MTBE) and 2 mL of NaCl (2.5 %, w/v). After centrifugation at 3300 rpm for 5 min (Rotofix 32A, Hettich), the cutin monomers were recovered in the MTBE supernatant, which was then washed once with 2 mL of saline buffer (Tris 100 mM, NaCl 0.9 % w/v). For wax and cutin extracts, derivatization by sylilation, GC−MS identification and GC−FID quantification were performed as described by Bourdenx et al. (2011) and Domergue et al. (2010), respectively.

Fruit maturity monitoring

Bunch maturity was determined 2 times per week (separated by 1 or 2 days within each week) throughout the veraison stage by monitoring the proportion of pink and violet berries reflecting the onset of anthocyanin accumulation (Fig. 1C). Mid-veraison was estimated according to a linear relationship as the date when 50 % of the berries were ripe (violet). Every berry was identified upon manifesting a violet (V) or pink (P) color on the 10th (V1, P1), 16–17th (V2, P2) and 23–24th (V3, P3) days (Fig. 1D) and defined hereinafter as the berry ripening stages. Furthermore, the total soluble solids (TSS) content of fresh juice from randomly selected berries, *i.e.*, 8 to 14 berries, assessed individually, per ripening stage (Fig. 1E) was measured using a portable digital refractometer (ATAGO), which provided an estimate of the sugar content (Shiraishi, 1993). For the other samplings, 20 and 10 berries were collected per variety × temperature × sampling day in 2023 and 2024, respectively (with one exception on the 13th day in 2023, where 30 berries were taken, *i.e.,* 10 per green, pink and violet color).

Botrytis population and disease assessment

In 2023 and 2024, two medium/high aggressive *Botrytis cinerea* isolates were used, herein designated *Bc*1 (corresponding to the "P" isolate in Hastoy et al., 2023) and *Bc*2 ("MGF-5664") from the INRAE-SAVE collection (isolate history and characteristics are summarized in Table 1). The phenotypes of the *Bc*1 and *Bc*2 isolates were MIII (sporulating weakly) and MII (sporulating profusely), respectively (Martinez et al., 2003). These isolates were cultivated on solid malt agar (malt 1.5 %, agar 2 % w/v) and transplanted every 1–2 weeks onto fresh medium before inoculation. In both years, on the 28th day (or 22 days after the 6-d HS; Fig. 1F), berries with attached pedicels were sampled randomly per ripening stage (V1 to P3), weighed and placed laterally on a grid in a moist incubation chamber exactly as described by Deytieux-Belleau et al. (2009) but without rinsing or disinfecting the surface (Supplemental Figure 2A). Inoculations were performed on up to 20 berries in 2023 and up to 60 berries in 2024 for every unique combination of variety, temperature, and ripening stage (with the exception that only the CS was tested in 2024). The following day, inoculation was performed by placing a mycelial plug (ø 4 mm) from a 1-week-old culture, with the mycelium in contact and facing the equatorial zone of the berry. The proportions of the berry surface colonized by low- and high-density mycelia (expressed in %), as well as the sporulating area (Supplemental Figure 2B), were visually evaluated at 6, 9, 13 and 16 days post-inoculation (dpi). Considering that the assessment was based on visual observation, proportions were graded on a scale of 0 to 100 % with a 5 % step. With the following formula, the estimated surface was calculated as a more robust parameter, integrating two fungal densities and giving more weight to high density according to factors of 1.5 and 3 for the mycelial and sporulating surfaces, respectively (based on

Table 1
Origin and type of *Botrytis cinerea* isolates used in this study. Indication of harvested year, site, variety and organ. Mycelial, sporulation and sclerotia phenotype on malt agar medium and associated class type according to Martinez et al. (2003). Reference reports use in previous study.

Strain	Year	Site	Variety	Organ	Mycelium	Sporulation	Sclerotia	Type	Reference
*Bc*1 ("P")	2020	Château de Mons (Caussens, Gers, Occitanie, France)	Baco blanc	Berries	Mycelial masses	–	–	MIII	Hastoy et al. (2023)
*Bc*2 ("MGF-5664″)	2024	Grande Ferrade (Villenave d'Ornon, Gironde, Nouvelle aquitaine, France)	Merlot	Berries	Aerial	+	–	MII	

symptom observations; Supplemental Figure 2C):

$$Estimated\ surface\ (\%) = \frac{low\ density\ +\ density\ factor \times high\ density}{density\ factor}$$

The area under the progressive curve (AUDPC) of both integrated parameters, calculated by the sum of trapezes under the curve (Simko and Piepho, 2012), was used to assess mycelium and sporulation progression over time.

Berry metabolite extraction

Targeted and untargeted metabolomic analyses were performed on five biological replicates of four seedless berries ($n = 5$) for each condition in 2023. Each berry was collected on the 29th day, stored one day in a moist incubation chamber as for the *B. cinerea* pathogeny test, but then directly snap frozen in liquid nitrogen and stored at −80 °C until freeze-drying (Fig. 1G). Metabolites extraction was conducted with 10 mg of lyophilized seedless berry material by a robotized extraction method developed at the Bordeaux Metabolome Facility (https://metabolome.cgfb.u-bordeaux.fr/en, Villenave d'Ornon, France), according to an ethanol fractionation protocol (Luna et al., 2020). The ethanol extracts were used to analyze the contents of fructose, glucose, malate, free amino acids, and polyphenols and for metabolic profiling, while the protein and cell wall contents were determined in the corresponding berry pellets.

Untargeted metabolomics profiling

The ethanol extracts were screened for untargeted metabolic profiling with a Vanquish (Thermo Fisher Scientific) system coupled with a Q Exactive Plus mass spectrometer (Thermo Fisher Scientific) at the Bordeaux Metabolome Facility. Separation was performed by injecting one microliter sample on a Phenomenex Luna Omega Polar C18 column (50 × 2,1 mm, 1,6 µm) at 40 °C with solvent A (0.1 % formic acid in water) and solvent B (0.1 % formic acid in acetonitrile) at a flow rate of 0.5 mL/min; the gradient was 0–7.5 min, 1–36 % B; 7.5–8.5 min, 36–95 % B; 8.5–10 min, 95 % B; and 10–12 min; 1 % B. The system was equipped with a heated electrospray ionization (HESI) source, and the ionization parameters were set as follows: negative mode, spray voltage: 3000 V, sheath gas: 45 au, aux gas: 15 au, capillary temperature: 320 °C, probe heater temperature: 250 °C, S-lens RF level: 100 V. MS data were acquired in full-scan data-dependent MS/MS (dd-MS2) analysis with the following acquisition parameters: for full MS, resolution: 35,000 full width at half maximum (FWHM), automatic gain control (AGC) target: 3e6 ions, maximum injection time (IT): 100 ms, scan range: 70–1050 *m/z*; for dd-MS2: resolution: 17,500 FWHM, AGC target: 1e5, maximum IT: 50 ms, isolation window: 2 *m/z*, number of precursor ions (top N): 2, normalized collision energy: 15, 30 and 40 V.

Targeted biochemical phenotyping

Targeted analyses of fructose, glucose, malate, and free amino acid contents, total soluble proteins and total cell wall content were conducted on the HiTMe plateau at the Bordeaux Metabolome Facility. Fructose, glucose, malate and free amino acid measurements were based on coupled enzyme assays (Luna et al., 2020). Assays were prepared in 96-well microplates with Starlet pipetting robots (Hamilton). The absorbance was read at 340 nm for fructose and glucose determination, and at 570 nm for malate determination with an MP96 microplate reader (SAFAS). Measurement of the amino acids was determined by fluorescence at 405 nm/485 nm. The protein content of the berry pellet resuspended in 100 mM NaOH was evaluated via the Bradford assay (Bradford, 1976), and the total cell wall content was determined by weighing the pellet after consecutive washing steps with 500 mM NaOH and water. Polyphenol quantification was performed with the same instrumental conditions used for untargeted metabolomic profiling by comparison with a calibration curve built with standards in the range of 0.029–14,93 mg/L. All compounds were quantified with the corresponding standard, except procyanidins B3 and B4, cis-piceid and cis-ε-viniferin, which were quantified as procyanidins B1 and B2, trans-piceid and trans-ε-viniferin, respectively. The software used for peak extraction and quantification was Xcalibur (Thermo version 4.6.67.17). All results are expressed as milligrams of compounds per gram of seedless berry (dry weight; DW).

Processing of metabolomic datasets

The raw LC–MS data were processed with MS-DIAL software v.4.9 (Tsugawa et al., 2015) with optimized parameters (MS1 tolerance: 0.008, MS2 tolerance: 0.025, minimum peak height: 30,000, retention time (RT) tolerance: 0.5, blank ratio: 5), which yielded 14,849 detected RT–*m/z* pairs. RT correction was also applied in MS-DIAL, and metabolomic signals were normalized by the QC samples injected every 11 samples, followed by a lowess and methylvanillate (internal standard) normalization. After data curation (blank check, SN > 10, coefficient of variation in quality controls < 30 %), we retained 4437 final features for further chemometric analysis. MS-DIAL annotation of metabolic features was performed with two in-house natural product databases: one from MetaboHUB (AgroMIx, Toulouse, France) and the other from the Bordeaux Metabolome Facility (ISVV, Villenave-d'Ornon, France). In addition, InChiKeys of annotated features were used in the ClassyFire batch (Djoumbou Feunang et al., 2016) to provide an automated structural ontology of chemical entities. Untargeted metabolomics data were normalized by the sum of total signals and by weight before performing multivariate and univariate statistical analyses. The extraction blanks, standards, and QC samples were discarded for clarity of visualization.

Skin condensed tannin extraction and assays

In 2023, condensed tannin analyses were performed using −20 °C-stored berries sampled 24 days after 6-d HS (Fig. 1H). For each sample, the skins from 10 berries were carefully peeled on ice, snap frozen in liquid nitrogen and crushed into powder with a cryogrinder (Freezer Mill 6875D, SPEX SamplePrep) prior to storage at −20 °C. All ripening stage × variety × temperature combinations were represented by 5 replicates, each of which originated from skin powder of 10 berries (with the exception of the M berries at ripening stages V1, P1 and V2 subjected to both temperatures owing to an insufficient number of available berries at the sampling time). Condensed tannins were extracted from 0.2 to 0.8 g of frozen skin powder according to the method outlined by Gagné et al. (2006) and filtered through a Falcon

filter (100 μm). Tannins were quantified by spectrophotometry according to the Bate–Smith reaction, *i.e.,* partial transformation of flavanol chains or procyanidins into cyanidins in heated acidic solution. As described by Pañitrur-De La Fuente et al. (2020), the assays were performed with 0.05 mL of extract mixed with 3 mL of HCL and 2.950 mL of water. Optical density (OD) at 550 nm was measured with a SPECTROstar Nano (BMG LABTECH, Champigny-sur-Marne, France) spectrophotometer in flat-bottom 96-well microplates (Microlon 200, Greiner Bio One) filled with 250 μl/well (technical replicates: 4 wells/plate/sample, 2 plates/sample). The tannin concentration was calculated from the difference in OD between heated and unheated solutions (ΔOD) according to the method outlined by Pañitrur-De La Fuente et al. (2020) and considering the dilution factor (4) as well as a correction based on a positive control run tested on all plates:

$$Tannins\ (mg/g\ \mathrm{FM}) = 4 \times 76.35 \times \frac{sample\ \Delta OD_{plate\ i}}{correction\ factor\ (cf)} \times \frac{1}{2 \times FM} \quad \text{where } cf = \frac{control\ \Delta OD_{plate\ i}}{control\ \Delta OD_{plate\ 1}}$$

Data and statistical analyses

Data analysis was performed with R (v4.4.2; R Core Team, 2024) and RStudio (v2024.12.0; RStudio Team, 2024). Data frame manipulation was conducted with the R packages "dplyr" (v1.1.4; Wickham et al., 2023), "tidyr" (v1.3.1; Wickham et al., 2024b), "stringr" (v1.5.1; Wickham, 2023) and "reshape2" (v1.4.4; Wickham, 2020, 2007). Graphics were generated with the R package "ggplot2" (v3.5.1; Wickham, 2016; Wickham et al., 2024) compiled with others according to chart requirements, namely, "ggpubr" (v0.6.0; Kassambara, 2023), "ggpattern" (v1.1.3; FC et al., 2024), "geomtextpath" (v0.1.5; Cameron and Brand, 2025), "ggmagnify" (v0.4.1; Hugh-Jones, 2024), "ggdist" (v3.3.2; Kay, 2024; Kay and Wiernik, 2024), "ggsignif" (v0.6.4; Ahlmann-Eltze and Patil, 2022, 2021), "ggrepel" (v0.9.6; Slowikowski et al., 2024), "ggVennDiagram" (v1.5.2; Gao et al., 2024) and "extrafont" (v0.19; Chang, 2023), and assembled with "gridExtra" (v2.3; Auguie and Antonov, 2017). Each box plot means, medians, interquartile range (IQR) are indicated by diamond, bold line, and rectangle, respectively. Whiskers indicate the most extreme values between the nearest quartile and 1.5 × IQR, beyond which outliers are represented by empty circle. AUDPC values were calculated with the R package "agricolae" (v1.3-7; de Mendiburu, 2023) according to the trapezoidal integration method described in Simko and Piepho (2012).

For statistical analysis, parametric assumptions were tested on raw values for pairwise comparisons and on model residuals for multiple comparisons (Kozak and Piepho, 2018). Normality was checked graphically, *i.e.*, with histograms and normal QQ plots for pairwise and multiple comparisons, respectively, and additionally tested with the Shapiro–Wilk test (from R base); both checks were performed within each group for pairwise comparisons. Variance homoscedasticity was verified with Levene's test from the R package "car" (v3.1–3; Fox et al., 2024; Fox and Weisberg, 2018). Pairwise comparisons were performed with Student's *t*-test or the Wilcoxon rank sum test (both from the R base) depending on whether the assumptions were validated (null hypothesis accepted) or rejected, respectively (Krzywinski and Altman, 2014). When the residuals met the assumptions, analysis of variance (ANOVA) was performed on the linear model, followed by Tukey's honest significant difference (HSD) test (both from the R base). Otherwise, non-parametric Kruskal-Wallis rank sum test (from R base) was performed, followed by Dunn's test (Agbangba et al., 2024) adjusted by the Bonferroni method with the R package "FSA" (v0.9.6; Ogle et al., 2025). Multiple significant differences are displayed with different letters with the R packages "multcompView" (v0.1–10; Graves et al., 2024) and "rcompanion" (v2.4.36; Mangiafico, 2024) for Tukey HSD and Dunn's test, respectively. Pairwise significant differences (from pairwise comparisons or two-factor comparisons by the Tukey HSD test) are displayed by *. All null hypotheses were rejected according to a 5 % risk threshold. Ridge, LASSO and Elastic-net models were constructed in R with the glmnet package (v 3.0-2; Friedman et al., 2010; Tay et al., 2023) to identify potential links between the detected metabolic markers and resistance to fruit pathogens. This top-down modeling approach was used to predict 2023 mycelium AUDPC values on the basis of the detected metabolic markers (not including the 2024 dataset, which was overfitted due to a single variety tested). Stratified sampling was performed with a random selection of 75 % of the individuals used to construct the models and by using the remaining 25 % to test the quality of the prediction. This process was performed 100 times for each dataset to address the random selection of the training and validation sets. Tenfold cross-validation was repeated 3 times in the construction of the models to decrease overfitting, and the mean square error was used to select the best models during the training step, based on a grid search over 40×40 combinations of the two penalization parameters (α and λ), with α values distributed between 0 and 1. The quality of the models was assessed on the basis of the coefficient of determination (R^2) between measured and predicted values in the test set. Thus, the variables occurring the most (50 %) in the models were considered as the most stable predictors of resistance to *B. cinerea* infection.

Results

The heated airflow device generated a 10 °C increase at the bunch level, which was associated with long-lasting drying of the air

The heated air stream was blown 8 h daily (8 a.m. to 4 pm.) on CS and M herbaceous bunches during a 6-d HS period. This condition is hereafter referred to as HS and is always compared with ambient airflow (CTRL).

Regardless of year, wherever the temperature was monitored, the HS condition significantly increased the average temperature to a range of 32.6–35 °C during the airflow period (vs. 23.1–24.9 °C for CTRL). In comparison to their respective CTRL (for each sensor and each year), the temperature elevation correspond to an increase in the air surrounding the bunch of 9.3 °C in 2024 and an increase in berry flesh of 10.1 °C and 10.5 °C in 2023 and 2024, respectively (Fig. 2A). Moreover, the VPD in the HS conditions was 2.3 kPa greater than that in the CTRL treatment (Fig. 2B). Although the temperature was similar during each period flanking the airflow, *i.e.,* morning (00:00–08:00): 17.6–19.2 °C, evening (16:00––00:00): 21.9–25.9 °C (Fig. 2A), a slightly higher VPD (+ 0.6 kPa) persisted in HS condition over the evening (Fig. 2B). Indeed, the temperature drop occurred almost immediately after HS (Supplemental Figure 2A), whereas a significant VPD difference between the CTRL and HS conditions persisted up to 6 h after HS ended (Supplemental Figure 2B). During the airflow period, the temperature and VPD under the HS conditions were always greater than those under the CTRL conditions (Fig. 2C, D), but while the temperature reached a maximum plateau within 2–3 h (at ≃ 35 or 32 °C in 2023 and 2024, respectively; Fig. 2C), VPD progressively increased until the end (Fig. 2D).

Therefore, bunches were subjected for 6-d to a daily 8-h 10 °C temperature increase associated with progressive air drying, which

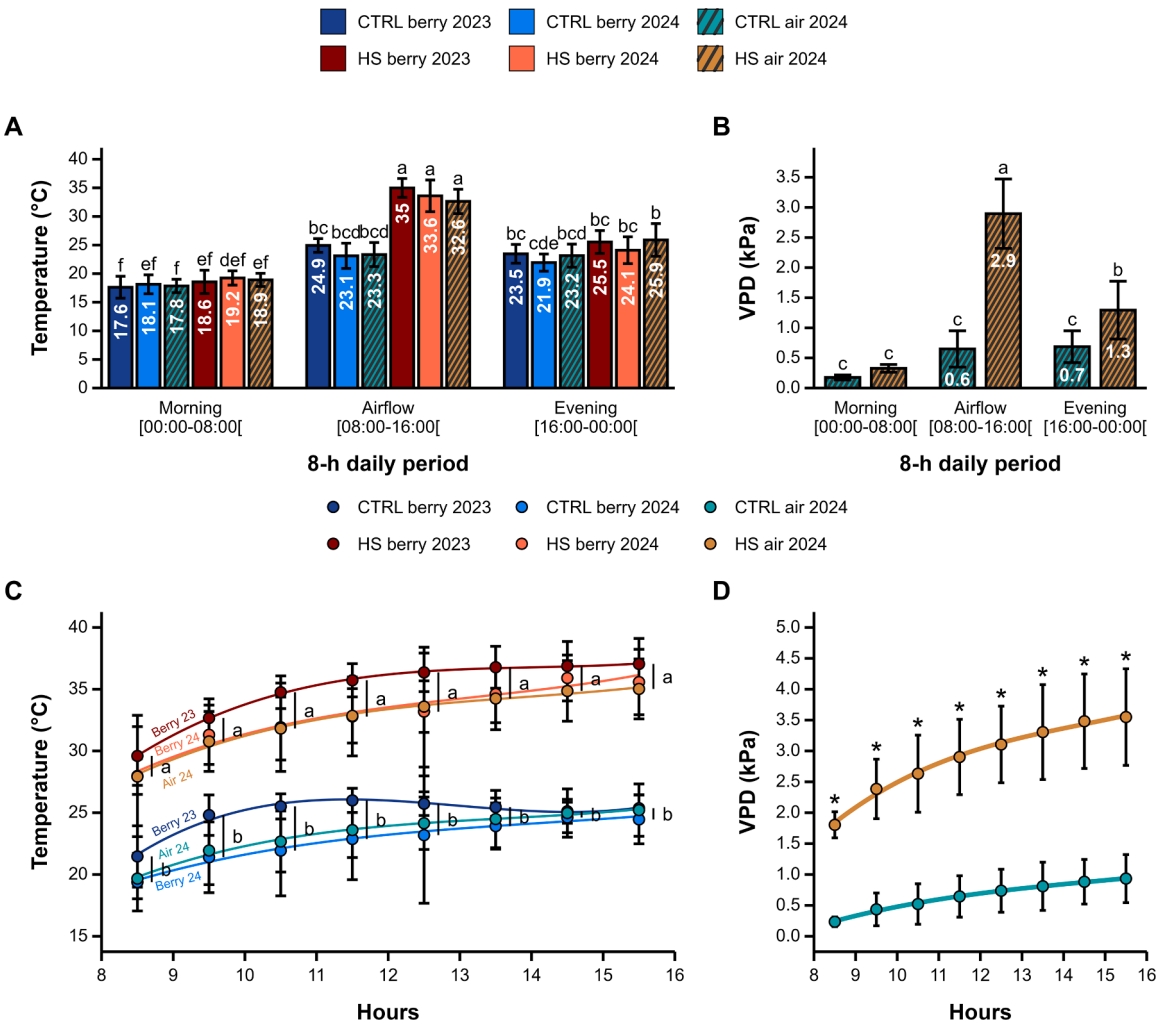

Fig. 2. Heat stress (HS) and control (CTRL) conditions applied on herbaceous bunch during the 6-d HS. Berry flesh temperatures were monitored in both years while air temperature and VDP around bunches were estimated only in 2024. (A, B) Daily average temperature (A) and VPD (B) per 8-h period. (C, D) Temperature (C) and VPD (D) evolution per 1-h interval only during the airflow exposure. Unwritten means < 0.5. Curves represents best fitted model for temperature (CTRL berry 2023 : $\gamma = -120 + 34x - 2.7x^2 + 0.068\times^3$, adjusted R^2 (R_{adj}) = 0.53; CTRL berry 2024 : $\gamma = -20 + 8.5x - 0.57x^2 + 0.013\times^3$, $R_{adj} = 0.46$; CTRL air 2024 : $\gamma = -39 + 13x + 0.95x^2 - 0.023\times^3$, $R_{adj} = 0.41$; HS berry 2023 : $\gamma = -70 + 23x + 1.6x^2 - 0.038\times^3$, $R_{adj} = 0.7$; HS berry 2024 : $\gamma = -40 + 16x + 1.1x^2 - 0.028\times^3$, $R_{adj} = 0.53$; HS air 2024 : $\gamma = -39 + 15x + 1.1x^2 - 0.025\times^3$, $R_{adj} = 0.53$) and for VPD (CTRL air 2024 : $\gamma = -1.7 + 0.3x - 0.0083x^2$, $R_{adj} = 0.36$; HS air 2024 : $\gamma = -3.7 + 0.88x - 0.027x^2$, $R_{adj} = 0.48$). Data are means per day ($n = 6$) ± CI. Different letters or * indicate significant differences according to Tukey HSD test (p-value < 0.05) following ANOVA on linear model 8-h periods × conditions × probes & years (A), 8-h periods × conditions (B), conditions × probes & years for each 1-h interval (C) and only conditions for each 1-h interval (D).

persisted until late evening.

HS applied at the herbaceous stage induced resistance against B. cinerea only for CS berries

Owing to the ontogenic resistance of green berries (Deytieux-Belleau et al., 2009), *B. cinerea* inoculations were performed *in vitro* on detached ripe berries 23 days after the 6-d HS. The poorly sporulating isolate *Bc*1 was tested on both varieties in 2023, whereas in 2024, only the susceptibility of CS berries was *de novo* checked with the highly sporulating isolate *Bc*2.

In 2023, mycelial growth on M berries remained the lowest throughout the experiment compared with that on CS berries (Fig. 3A). In addition, the progression of mycelium on M berries was unaffected by the HS treatment. In contrast, mycelial colonization of heat-stressed CS berries was clearly delayed and reached a much lower final level than that of the CTRL berries. These trends were significant at every dpi in 2023 but were only noticeable in 2024 (not statistically significant). Concerning sporulation progression, the *Bc*1 isolate used in 2023 sporulated too weakly to have any effect on M berries (Fig. 3B). Nevertheless, sporulation on CS berries was systematically lower following HS in both 2023 and 2024, even if it was not significant at each dpi.

When looking at the AUDPC for each berry ripening stage (Fig. 1D; Supplemental Figure 4A), only a few significant differences between CTRL and HS berries within the same maturity stage were revealed, *e.g.,* HS increased resistance against *Bc*1 mycelial growth in CS at P1 and V3 (Supplemental Figure 4B). Splitting the AUDPC according to maturity stage impeded the detection of a clearly significant pattern, although heated CS berries tended to be mostly more resistant than CTRL berries for most maturity stages (Supplemental Figure 4). We then investigated the main effects of the varieties/isolates, the conditions and the berry ripening stages with ANOVA on the AUDPC of mycelium and sporulation (Table 2). Importantly, a significant HS effect was shown on the mycelial AUDPC ($\eta 2 = 0.05$), although the varieties & isolates effect explained more of the variance than any other factor ($\eta 2 = 0.29$). This was confirmed in 2023 by a noteworthy decrease in *Bc*1 mycelial AUDPC in heated CS compared with that in CTRL, which reached a level

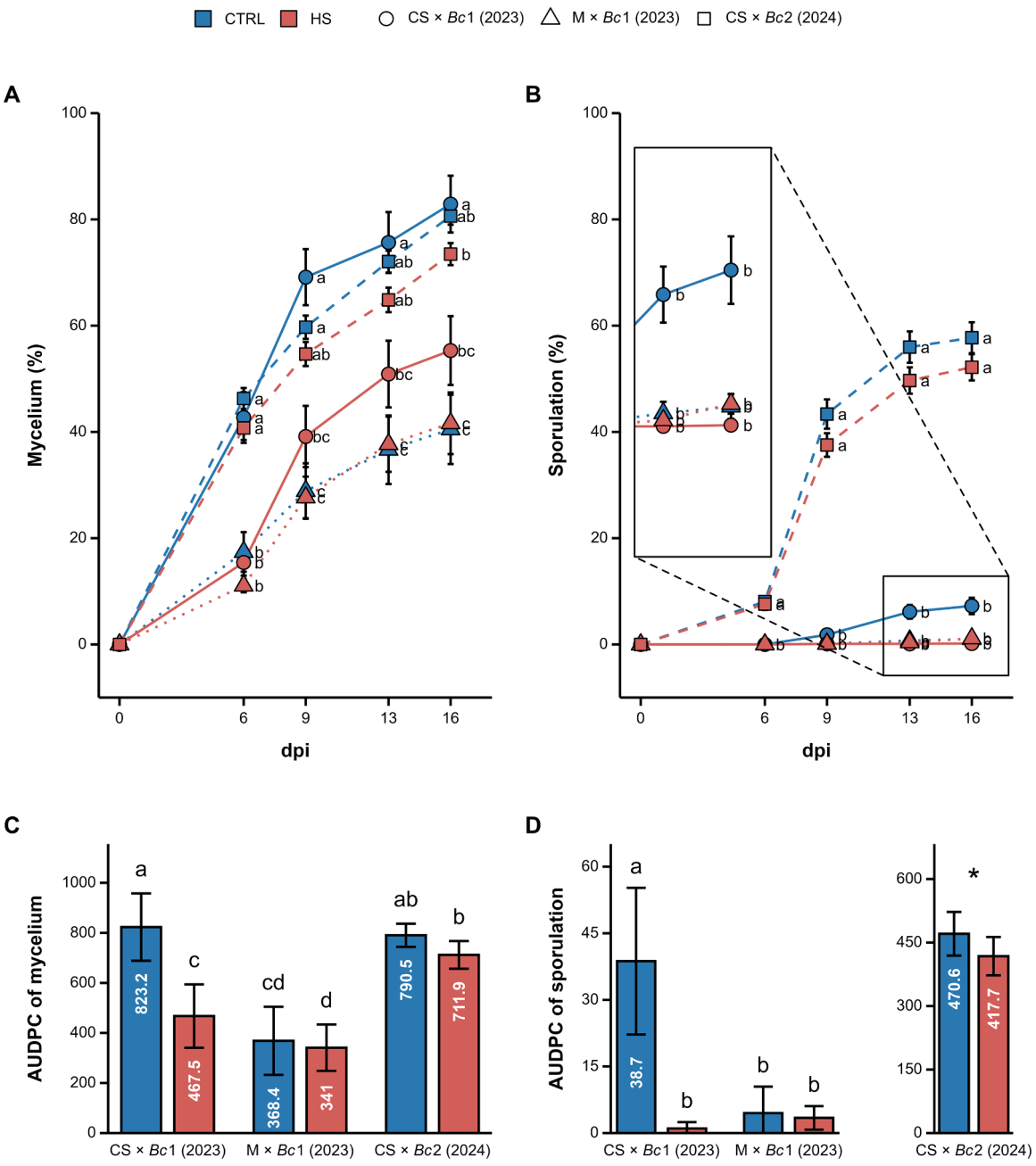

Fig. 3. *In vitro* evaluation of *Botrytis cinerea* progression on the surface of Cabernet Sauvignon (CS) and Merlot (M) berries submitted to control (CTRL) or heat stress (HS) conditions. Inoculations were performed on both varieties in 2023 and only on CS in 2024 with *Bc*1 or *Bc*2 isolate, respectively. (A, B) Average progression of mycelium (A) and sporulation (B). (C, D) AUDPC of mycelium (C) and sporulation (D). Unwritten means < 5. Data are means of symptoms on at most 5 berries per variety × condition × maturity ($n = 22$–46) ± SE for line plot (A, B) or ± CI for bar plot (C, D). Different letters displayed in line plot indicate significant difference at each dpi according to Dunn's test associated with Bonferroni correction following significant Kruskal-Wallis test (p-value < 0.05; A, B). Different letters or * displayed in bar plot indicate significant difference according to Tukey HSD test (p-value < 0.05) following ANOVA on linear model varieties & isolates × conditions × ripening stages for mycelium (C) or conditions × ripening stages for sporulation in 2024 (D). Non-parametric statistics as used for line plot were applied for AUDPC of sporulation in 2023 due to the noncompliance with assumptions.

close to the high resistance observed in M (Fig. 3C). For *Bc*1 sporulation AUDPC, similar varietal and HS-induced resistances were also highlighted in 2023 by a nonparametric test (Fig. 3D). Although *Bc*2 mycelium AUDPC was not significantly different between both conditions in 2024, a significant HS effect ($\eta 2 = 0.03$) on sporulation AUDPC, resulting from the greater resistance of heated CS (Fig. 3D), was observed (Table 2). The berry maturity stage clearly played a key role in the interactions with the other factors (Table 2).

Taken together, these tests revealed heat-enhanced resistance only for CS, which was reflected by both restricted mycelium progression and reduced sporulation.

Key physiological features linked with maturity were insensitive to HS

The bunch veraison status was monitored to determine whether resistance against *B. cinerea* could indirectly be linked to a delay in ripening caused by HS (Supplemental Figure 5A).

Berry color began to change a few days after the 6-d HS treatment until the bunches had almost completely ripened just before the inoculation, which did not reveal any significant difference between the HS

Table 2
ANOVA of the effect of isolates & varieties × temperature conditions × berry ripening stages on AUDPC of mycelium from both year and temperature conditions × berry ripening stages on AUDPC of sporulation from 2024.

AUDPC	Factor	Df	SS	MS	*F*	*P*	η2
Mycelium (2023-2024)	Isolates & varieties	2	4621420	2310710	117.621	< 2e-16***	0.29
	Conditions	1	882599	882599	44.926	4.23e-10***	0.05
	Ripening stages	5	1579474	315895	16.080	1.36e-12***	0.1
	Isolates & varieties × Conditions	2	797318	398659	20.293	1.70e-08***	0.05
	Isolates & varieties × Ripening stages	10	2660512	266051	13.543	< 2e-16***	0.17
	Conditions × Ripening stages	5	675903	135181	6.881	8.61e-06***	0.04
	Isolates & varieties × Conditions × Ripening stages	10	2038197	203820	10.375	4.37e-13***	0.13
	Residuals	145	2848587	19645			0.18
Sporulation† (2024)	Conditions	1	62227	62227	4.153	0.04499*	0.03
	Ripening stages	5	293086	58617	3.912	0.00326**	0.13
	Conditions × Ripening stages	5	775393	155079	10.351	1.29e-07***	0.34
	Residuals	77	1153629	14982			0.51

Df: Degree of freedom, SS: Sum of Squares, MS: Mean Squares, *F*: F-value *P*: P-value, η2: effect size. * *p*-value < 0.05, ** *p*-value < 0.01, *** *p*-value < 0.001. The redder the color, the closer the value of η2 is to 1.
†exclusion of 2023 sporulation data from model due to the noncompliance with assumptions, related to high low-values frequency (65 % of values = 0).

and CTRL conditions (Supplemental Figure 5B). This noteworthy outcome was confirmed by mid-veraison estimation, which appeared to depend on the variety rather than on the HS treatment in 2024 (Fig. 4A). In addition, 78 % of the mid-veraison disparity was not explained by variety, year or condition (Table 3), highlighting the asynchronous development of the fruiting cuttings.

Finally, the results of the maturity assessment were also supported by measuring the TSS content that reflects sugar accumulation in berry juice (Shiraishi, 1993). As shown in Fig. 4B, total sugar content increased with bunch ripening but was similar under the HS and CTRL conditions. Green berry sugars remained low, *i.e.,* from an average of 3.8–6.5 °Brix, throughout the 6-d HS and gradually increased as the fruits became purplish, finally reaching an average range of 16.7–18.7 °Brix or 17.0–20.9 °Brix for CS and M, respectively.

Furthermore, the mass and volume of the berries used for pathogen assays were measured and estimated, respectively. These two highly correlated parameters were influenced neither by HS nor by variety (Fig. 4C, D), even when each maturity level was considered separately (Supplemental Figure 6A, B). A significant difference was detected only between the 2 years of experimentation, with lighter and less voluminous berries in 2024 than in 2023.

Taken together, these results revealed that HS did not affect physiological traits related to the fruit ripening level, which suggested that other factors were responsible for the improved resistance against *B. cinerea* observed in CS.

Berries accumulated cutin monomers in cuticle in response to HS

The berry cuticle, made of wax and cutin, constitutes the first barrier encountered by *B. cinerea* in the early infection phases (González et al., 2016). Therefore, wax and cutin components were quantified from the 6-d HS to inoculation (Fig. 5). If the very same wax constituents and cutin monomers were found in all conditions (Supplemental Table 1), the contents of several cuticular component clearly differed according to the variety (CS or MS), and were affected by the condition (CTRL or HS).

Regardless of the conditions, waxes were more abundant in CS than in M (Fig. 5A), which was mainly related to the three major aliphatic wax classes, *i.e.,* alcohols, aldehydes and fatty acids (Supplemental Figure 7A, 8A). With respect to cutin, albeit less perceptible in terms of total quantities (Fig. 5A) or compound class quantities (Supplemental Figure 7B), most of the major cutin monomers were more abundant in M than in CS on the 27th day (Supplemental Figure 8B). Apart from a varietal difference in cuticle composition, the total amount of identified wax and cutin compounds was not significantly modified in heated berries compared with that in CTRL berries (Fig. 5A). Similarly, no effect of HS on the total quantity of the different compound classes was detected, although HS induced a nonsignificant overaccumulation of fatty acid waxes in CS on the 27th day (Supplemental Figure 7A) and dicarboxylic acid cutin monomers in both varieties (Supplemental Figure 7B).

To specifically evaluate differences in cuticular composition within the same variety (CTRL *vs.* HS) on the day preceding inoculation (*i.e.,* on the 27th day), volcano plot representations were then generated. The only wax compound that significantly varied in quantity was C26 fatty acid ethyl ester, which content slightly increased only in CS (Fig. 5B). This content of this compound was very low (representing less than 0.3 % of the total waxes), and following HS reached in CS a level similar to that of M (Fig. 5C). In terms of cutin monomers, C16:0 and C18:2 ω-hydroxylated fatty acids were increased by HS in both varieties (Fig. 5B). In addition, C16:0 ω-hydroxylated, dicarboxylic and dihydroxylated fatty acids significantly overaccumulated only in the HS-treated CS berries. Although the amounts of these cutin monomers increased in the HS-treated CS berries, they remained below those of the M berries regardless of the conditions applied, except for the C16:0 dihydroxylated fatty acids, which reached the same level (Fig. 5C).

Notably, in contrast to the very minor C26 fatty acid ethyl ester, these 5 cutin compounds accounted for 16–21 % of all cutin building blocks, suggesting that HS affected cuticular composition through the deeper layer of cutin rather than *via* surface waxes.

Skin condensed tannins were increased by HS depending on the ripening stage

Fungitoxic tannins provide an additional line of defense by impeding infection progression after *B. cinerea* has penetrated the cuticle (Deytieux-Belleau et al., 2009). In CS berries, the total quantity of condensed tannins in the skin was significantly increased by HS (Fig. 6A). This was mostly caused by significant overaccumulation observed notably at the V2 ripening stage (Fig. 6B). However, in this variety, no effect of the ripening stage was detected, which indicates that the basal amount of tannins was similar regardless of the ripening stage considered (Table 4).

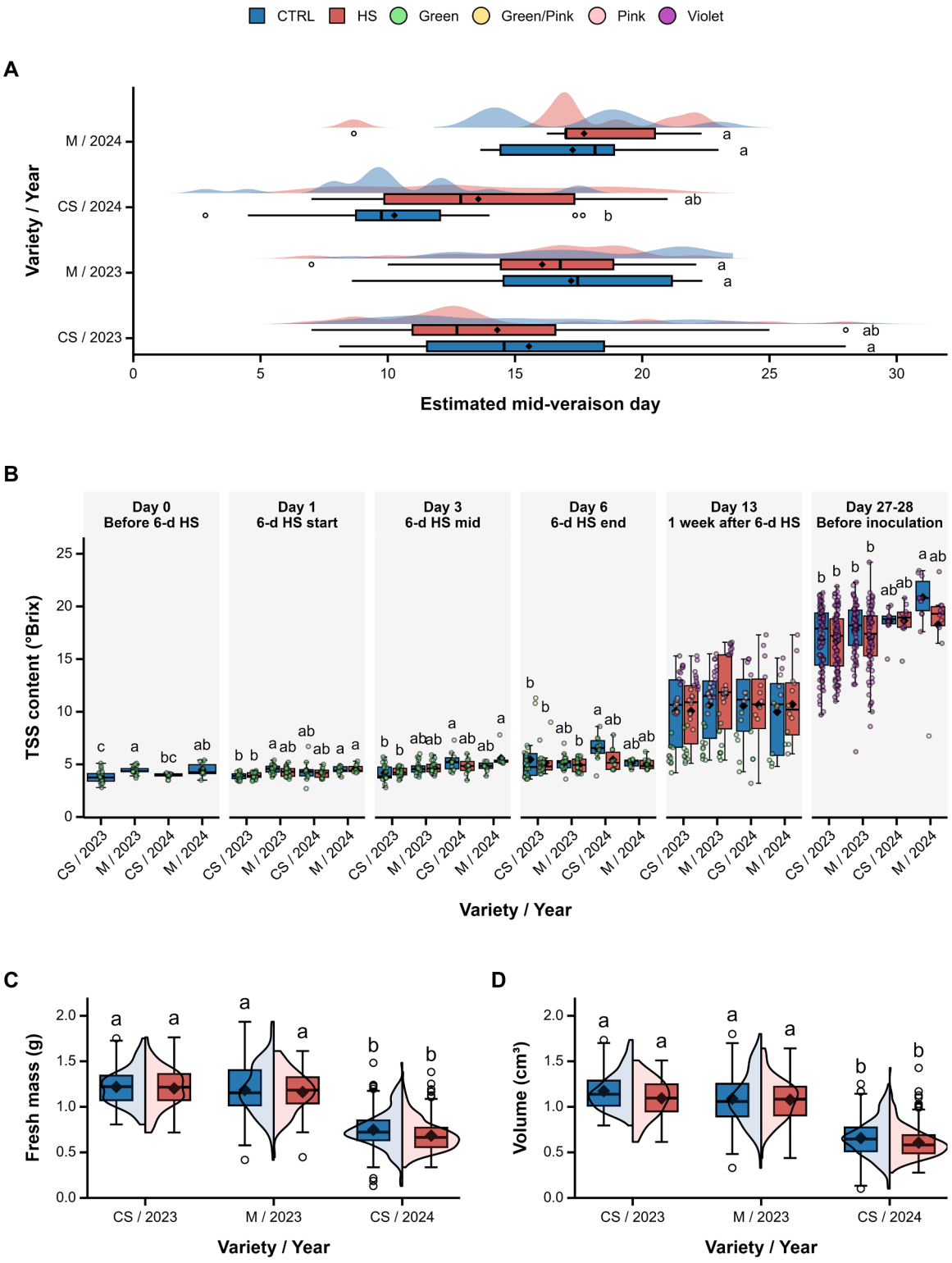

Fig. 4. Maturity monitoring of Cabernet Sauvignon (CS) and Merlot (M) grapes exposed to control (CTRL) or heat stress (HS) conditions. (A) Estimated bunches mid-veraison of each fruiting cutting ($n = 9$–22). Day 0 correspond to the day before 6-d HS beginning (23/05/2023 or 18/06/2024). Different letters indicate significant difference according to Tukey HSD test (p-value < 0.05) following ANOVA on linear model years × varieties × conditions. (B) Kinetics of total soluble solids (TSS) content of randomly sampled berries ($n = 9$–88). Colors refer to those of sampled berries. (C, D) Fresh mass (C) and volume (D) of tested berries *prior* inoculation ($n = 109$–230). (B, C, D) Different letters indicate significant difference according to Dunn's test associated with Bonferroni correction following significant Kruskal-Wallis test (p-value < 0.05). Unrepresented significance indicates no difference between means of the corresponding kinetic sampling.

Table 3
ANOVA of the effect of years × varieties × conditions on estimated mid-veraison.

Physiology	Factor	Df	SS	MS	*F*	*P*	η2
Mid-veraison	Years	1	124	124	6.009	0.0156	0.037
	Varieties	1	344.4	344.4	16.691	7.77e-05***	0.104
	Conditions	1	5.7	5.7	0.274	0.6013	0.002
	Years × Conditions	1	112.2	112.2	5.437	0.0213*	0.034
	Years × Varieties	1	105.7	105.7	5.123	0.0253*	0.032
	Varieties × Conditions	1	9.7	9.7	0.468	0.4953	0.003
	Years × Varieties × Conditions	1	16.5	16.5	0.801	0.3724	0.005
	Residuals	126	2599.7	20.6			0.784

Df: Degree of freedom, SS: Sum of Squares, MS: Mean Squares, *F*: F-value *P*: P-value, η2: effect size. * p-value < 0.05, ** p-value < 0.01, *** p-value < 0.001. The redder the color, the closer the value of η2 is to 1.

The variety comparison, which was based on the shared maturity levels of both varieties—*i.e.,* starting to turn color at least two weeks after 6 days of HS—revealed a significantly greater tannin content in CS (Fig. 6C). Although the variety explained most of the tannin content (η2 = 0.47), the effect of the applied condition and ripening stage was significant (Table 4). The tannin content was significantly increased by HS in M within this ripening window, *i.e.,* P2, V3 and P3 (Fig. 6C). More specifically, tannins increased following HS for the two later maturity stages (P2 and V3), but the difference between the CTRL and HS conditions decreased gradually with the advancement of ripeness until it became nonsignificant at the P3 stage (Fig. 6D).

Thus, condensed tannins were responsive to HS only when berries were exposed during a specific ripening period for both the CS and M varieties.

Berry metabolism remained altered 3 weeks after the end of HS

In addition to skin features, berry metabolism could have contributed to the heat-enhanced resistance observed in CS. To verify this hypothesis, the contents of the cell wall, proteins, amino acids, malate and sugary compounds, flavan-3-ols, flavonols and the stilbene family were investigated (Supplemental Table 2). The berry metabolome was also further studied through an untargeted analysis.

A substantial number of these metabolites were clearly differentiated between varieties according to the conditions (Fig. 7A). Interestingly, under both conditions, CS accumulated more malate and phenolic cis-caftaric acid, whereas both stilbene cis-resveratrol and δ-viniferin were oversynthesized in M. In addition, four stilbenes (pallidol, isohopeaphenol, and ε-viniferin isomers 1 and 2) and six flavan-3-ols (catechin, epicatechin, epicatechin gallate, procyanidin B2, B4 and isomer 2) were more abundant in M at the basal state (CTRL). In CS berries, the contents of two targeted metabolites were modulated by HS, *i.e.,* the overaccumulation and underaccumulation of glucose and amino acids, respectively (Fig. 7B). Nevertheless, heated M berries presented significant decreases in amino acids, proteins, four stilbene compounds, *i.e.,* cis-resveratrol, piceatannol, δ-viniferin and ε-viniferin isomer 2, and the flavan-3-ol epigallocatechin (Fig. 7B). The heat-reduced content of amino acids observed within both varieties was more pronounced in M than in CS, similalrly to the significant decreases in other compounds observed solely in this variety (Fig. 7C). Furthermore, stilbenes exhibited a common pattern, with higher amounts in CTRL M berries, which were diminished by HS and reached levels close to those of CS berries regardless of the condition applied.

Untargeted analysis confirmed the marked difference in metabolism between the two varieties (Supplemental Figure 9A). Furthermore, this analysis provided a deeper insight into the global effect of HS on the metabolite contents within each variety (Supplemental Figure 9B). M metabolism was far more responsive to HS than CS metabolism, with almost 2- or 4-fold more underaccumulated and overaccumulated untargeted metabolites, respectively (Fig. 8A). In both varieties, 5 and 27 compounds were jointly increased or decreased by HS, respectively. Among the top 8 represented metabolite classes, 5 classes, *i.e.*, "organooxygen compounds", "carboxylic acids and derivatives", "benzene and substituted derivatives", "fatty acyls" and "flavonoids", were both underaccumulated and overaccumulated following HS, regardless of variety (Fig. 8B). Although they underaccumulated in both varieties, "isoflavonoids" and "quinolines and derivatives" compounds were also induced by HS only in M and CS, respectively. Similarly, heat-induced compounds in both varieties included a "prenol lipids" class, which was also represented as less accumulated compounds in heated M berries.

Within CS, the specific classes that only accumulated less following HS corresponded to "glycerophospholipids" and "depsides and depsidones", whereas the classes that overaccumulated after HS were "coumarins and derivatives", "indoles and derivatives", "saccharolipids" and "tannins". The predicted compounds and associated classes modulated by HS in CS are listed in Supplemental Table 3. Among these, HS reduced the content of 7 flavonoids, including pinocembrin, cyanidin and acacetin, whereas only two were stimulated, *i.e.,* 8-prenylnaringenin and 2,3-trans-3,4-trans-leucocyanidin. On the other hand, two tannin compounds accumulated solely after HS, *i.e.,* benzoic acid + 1O, 1MeO, O-Hex and [3,4,5-trihydroxy-6-[3-(4-hydroxyphenyl)prop-2-enoyloxymethyl]oxan-2-yl] 3,4,5-trihydroxybenzoate.

Taken together, these results highlighted the differences in metabolism between CS and M and the response to HS within each variety.

The prediction model for the 2023 dataset highlighted the close relationship between cutin and resistance against B. cinerea

To confirm the link between *B. cinerea* pathogenicity and berry metabolomes, Ridge, LASSO and Elastic-net models (later refered to as GLMs) were computed on AUDPC mycelium with waxes, cutin monomers, and target and untargeted metabolites from our 2023 dataset.

The occurrence of heat-induced overaccumulated waxes (C26 ethyl ester fatty acid) and cutin monomers (C16:0 dicarboxylic acid, C18:2 ω-hydroxylated fatty acid and C16:0 ω-hydroxylated fatty acid; Fig. 5B) confirmed their importance in mycelial AUDPC reduction (Table 5). Interestingly, these 3 cutin monomers were also more abundant in M (see Supplemental Figure 8B), and thus, are potentially linked to both varietal and HS-induced resistance. Other cuticular compounds that overaccumulated in M and in CS may explain the varietal resistance according to the negative and positive coefficients in the models, respectively: C30 alcohol, C28 aldehyde, C32 aldehyde, uvaol, C20 fatty acid, and C24 aldehyde within waxes and C18:1 dicarboxylic acid, C18:0

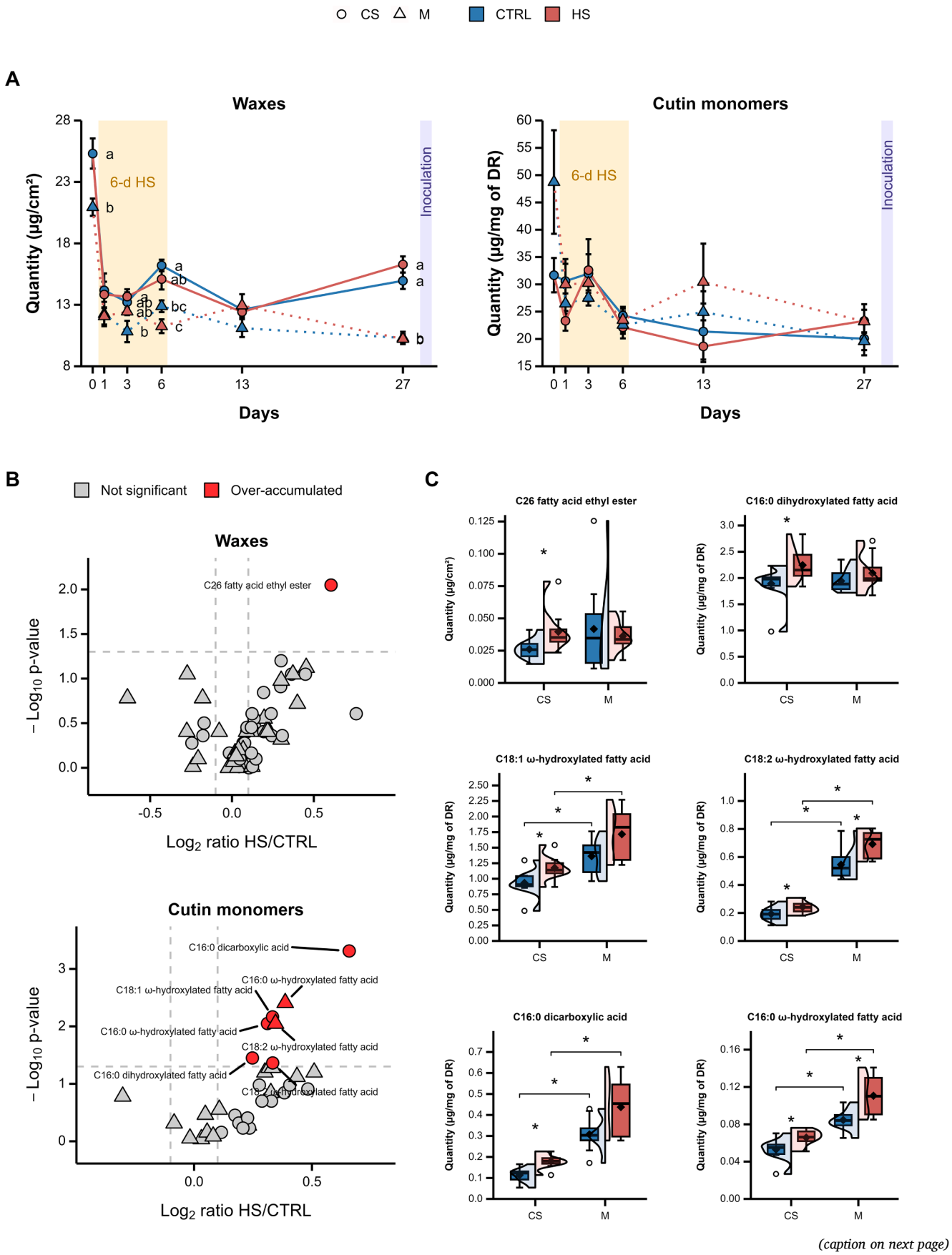

(caption on next page)

Fig. 5. Impact of control (CTRL) and heat stress (HS) conditions on the amounts of cuticular compounds from Cabernet Sauvignon (CS) and Merlot (M) berries. (A) Developmental kinetics of total wax and cutin monomers identified from the day before 6-d HS (23/05/2023 or 18/06/2024) until berries inoculation. Data are mean ± SE ($n = 10$). CS and M identified by solid and dotted line, respectively. Different letters indicate significant difference at each notation according to Dunn's test associated with Bonferroni correction following significant Kruskal-Wallis test (p-value < 0.05). Unrepresented significance indicates no difference between means of the corresponding notation day. (B) Volcano plot of modulation waxes and cutin monomers from berries sampled the 27th day. Each point corresponds to a compounds within the same variety. The x-axis represents the $\log_2$ ratio HS/CTRL of mean quantity of each waxes (µg/cm²) and cutin monomers (µg/mg of DR). The y-axis represents the -$\log_{10}$ p-value from Wilcoxon rank sum test. Labelled points corresponds to significant compounds modulated by HS (p-value < 0.05 and $-0.1 >$ $\log_2$ ratio > 0.1). (C) Quantity of each significant compounds. Significant pair-wise comparison from Wilcoxon rank sum test between CTRL and HS within the same variety and between CS and M exposed to the same condition are indicated by *.

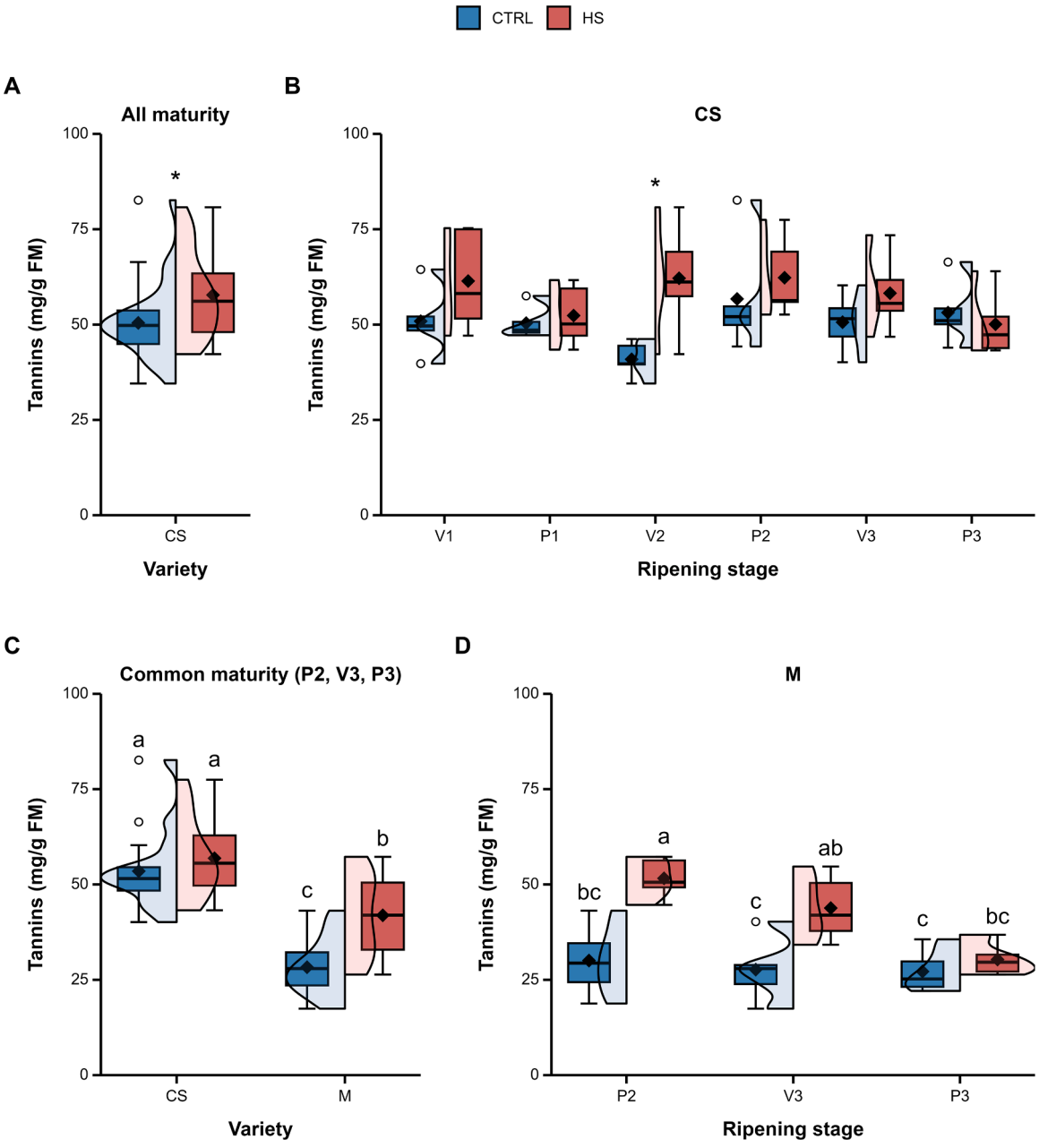

Fig. 6. Global condensed tannins content from Cabernet Sauvignon (CS) and Merlot (M) berries skin 24 days after exposition to control (CTRL) or heat stress (HS) conditions. (A) Global CS tannins at all ripening stages included (V1, P1, V2, P2, V3 and P3; $n = 30$). (B) CS tannins for each ripening stage ($n = 5$). (C) CS and M tannins at common ripening stages (P2, V3 and P3; $n = 15$) (D) M tannins at each ripening stage studied ($n = 5$). Each biological replicate (5 replicate per variety × condition × ripening stage) was from skin powders of 10 pooled berries. Significant pair-wise comparison from Student test between CTRL and HS within CS are indicated by *. Different letters indicates significant difference according to Tukey HSD test ($P < 0.05$) following ANOVA on linear model varieties × conditions + ripening stages (C) or conditions × ripening stages (D).

Table 4
ANOVA of the effect of varieties × conditions + ripening stages on tannins content for both varieties at P2, V3 and P3 ripening stage and varieties × conditions within each varieties.

Tannins	Factor	Df	SS	MS	*F*	*P*	η2
CS × M (P2, V3, P3)	Varieties	1	6050	6050	73.623	1.15e-11***	0.47
	Conditions	1	1082	1082	13.171	0.000632***	0.08
	Ripening stages	2	997	499	6.068	0.004195**	0.08
	Varieties × Conditions	1	393	393	4.781	0.033135*	0.03
	Residuals	54	4437	82			0.34
CS (V1, P1, V2, P2, V3, P3)	Conditions	1	803	803.2	8.085	0.00654**	0.12
	Ripening stages	5	538	107.7	1.084	0.38122	0.08
	Conditions × Ripening stages	5	859	171.7	1.728	0.14618	0.12
	Residuals	48	4769	99.3			0.68
M (P2, V3, P3)	Conditions	1	1389.6	1389.6	27.195	2.41e-05***	0.37
	Ripening stages	2	735.7	367.9	7.199	0.00355**	0.19
	Conditions × Ripening stages	2	448.2	224.1	4.386	0.02380*	0.12
	Residuals	24	1226.4	51.1			0.32

Df: Degree of freedom, SS: Sum of Squares, MS: Mean Squares, *F*: F-value *P*: P-value, η2: effect size. * *p*-value < 0.05, ** *p*-value < 0.01, *** *p*-value < 0.001. The redder the color, the closer the value of η2 is to 1.

dihydroxylated fatty acid, and C18:1 epoxylated ω-hydroxylated fatty acid within cutins (Table 5; Supplemental Figure 8). Since these models were well adjusted for the 2023 data ($R^2 = 0.70$ and 0.72 for waxes and cutin monomers, respectively), all others compounds that stand out as cuticular compounds were probably not linked to AUDPC solely in 2024, *i.e.,* as a consequence of an annual effect visible only in 2023 (therefore not significant in our previous analysis combining both years; see Fig. 5B).

With respect to the targeted metabolites, only the reduction in amino acids caused by HS was related to the decrease in AUDPC, as observed in CS (Fig. 7B). In addition, the GLM confirmed the strong link ($R^2 = 0.58$) between higher levels of metabolites and M resistance (catechin, cis-resveratrol, ε-viniferin isomer 1, epicatechin, isohopeaphenol, procyanidin isomer 2 and epicatechin gallate) or CS susceptibility (trans- and cis-coutaric acid; Table 5; Fig. 7A). Given the small number of samples in this analysis, further analyses are nevertheless required to confirm the link of other metabolites with AUDPC.

Surprisingly, the predictive untargeted metabolomic analysis allowed us to identify only 6 important compounds ($R^2 = 0.67$), and their normalized peak intensity, represented in Fig. 9, confirmed their relationship with the contrasting resistance phenotypes. Most of these compounds were related to both varietal and HS-repressed susceptibility, *i.e.,* pinocembrin, mono(2-ethyl-5-carbonyxpentyl) adipate, cyanidin-3,5-diO-glucoside and 2-hydroxybenzonitrile. The only compounds not predicted (unknown 9877) were uniquely associated with increased CS susceptibility compared with that of M. D-fructose 6-phosphate was the single untargeted compound that overaccumulated in the resistant phenotype, being HS-induced in CS but not reaching a level as high as in M.

Overall, the GLM confirmed the relationship between the phenotype observed with the accumulation of several metabolites potentially playing a role in resistance or susceptibility to *B. cinerea*.

Discussion

Depending on the cultivar and the region, early leaf removal (after fruit set, without effect on bunch compactness) overexposes bunches to wind and sunlight, reducing microclimate parameters favorable for *B. cinerea* establishment, such as relative humidity and duration of leaf wetness (Molitor et al., 2011; Pañitrur-De La Fuente et al., 2020; Würz et al., 2020). Our experimental setup was designed to measure the effect of a significant increase in the temperature of bunch microclimate at the end of the green/herbaceous berry stage, as observed following leaf removal in northern-hemisphere vineyards (Sternad Lemut et al., 2013), on subsequent Botrytis infection. In the context of global warming, more frequent and/or intense HS could challenge this practice at the early phenological stage, such as in the Bordeaux wine-growing region, where CS and M are among the most widely used cultivars (Gambetta and Kurtural, 2021; van Leeuwen et al., 2019). Our controlled conditions allowed us to mimic a temperature increase of 10 °C focused on bunches (Fig. 2A, C) and therefore a mostly thermal effect in the complex abiotic microclimate, *e.g.,* excluding the effect of sunlight exposure, which is known to affect berry metabolism (Ghiglieno et al., 2020; Torres et al., 2021). However, our system could not prevent changes in air relative humidity, which is directly linked to both temperature and ventilation, leading to slight changes in VPD (Fig. 2B, D; Gouot et al., 2019).

In grapevine, berry preformed defenses such as the cuticle or tannins are important determinant to prevent the success of *B. cinerea* first infection steps (Comménil et al., 1997; Deytieux-Belleau et al., 2009; Gabler et al., 2003). Conversely, others constituents or features, notably the presence of micro-pores and/or hexose exsudates at the berry surface, can be exploited by *B. cinerea* to bypass these first defenses (Gabler et al., 2003; Kretschmer et al., 2007). Overall, host fruit preformed skin features can enhance or hinder subsequent fungal colonization. Depending on their quantity and/or structure, host factors predisposing to tolerance can weight heavily in the balance, helping the host to take the lead and contain infection (Moerschbacher and Mendgen, 2000; Osbourn, 1996). On the contrary, factors predisposing to susceptibility can allow the fungus to overtake the host, without the preformed or induced defense being effective and/or not giving enough time for the host to respond effectively to the infection (Gorshkov and Tsers, 2022; van Schie and Takken, 2014). When heat-tolerance mechanisms interfere with the factors predisposing to tolerance or susceptibility this host balance can be disrupted by HS, and then reverse the outcome of disease (Shelake et al., 2024). The primary goal of this study was therefore to study the effect of HS on grape berry preformed barriers against *B. cinerea*.

Our first key finding was that a 6-d HS was sufficient to significantly

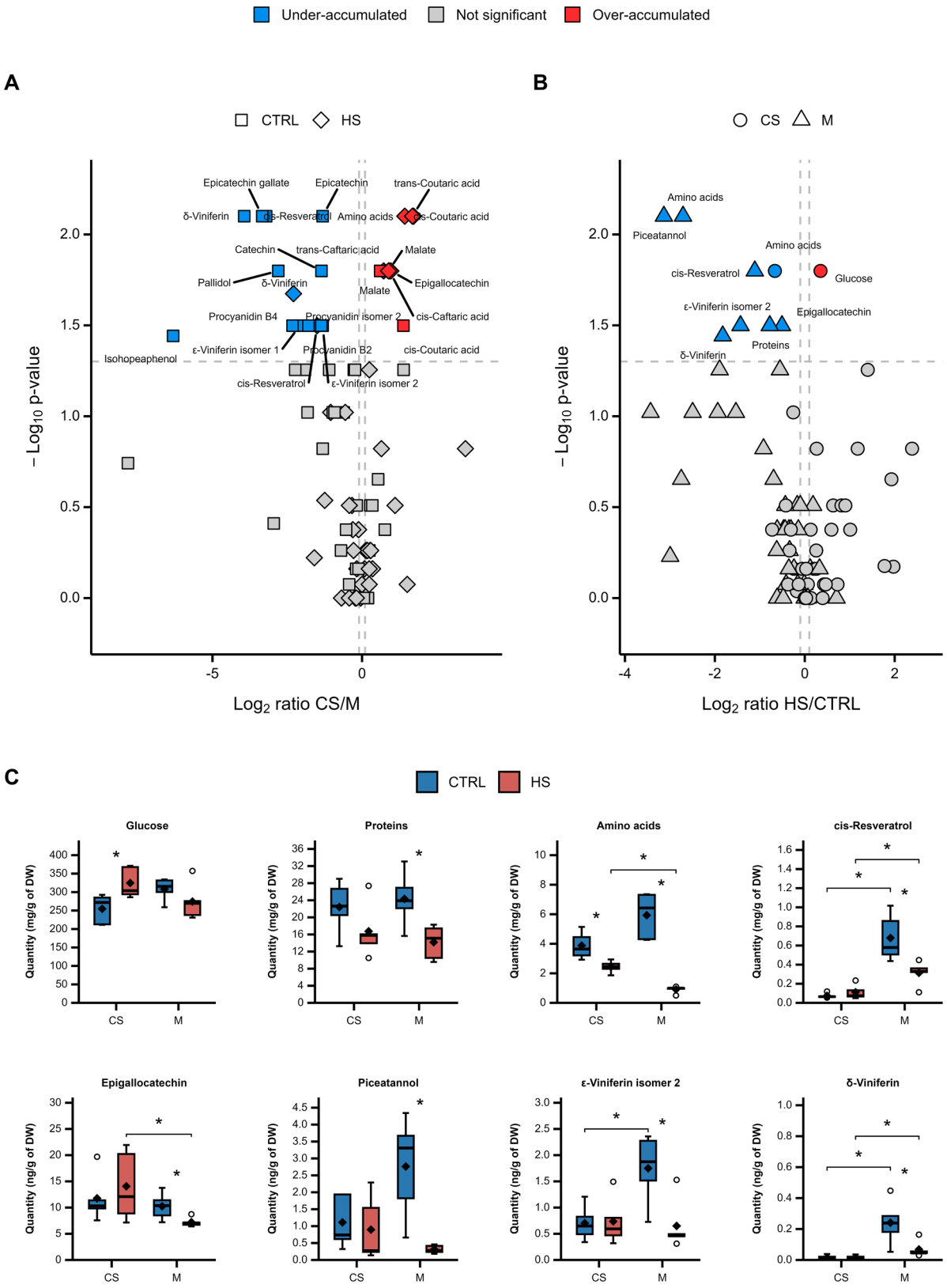

Fig. 7. Targeted metabolomic analysis of Cabernet Sauvignon (CS) and Merlot (M) berries 23 days after exposition to control (CTRL) or heat stress (HS) conditions. (A) Varietal difference, Cabernet Sauvignon (CS) *vs.* Merlot (M); (B, C) Condition difference, heat stress (HS) *vs.* control (CTRL). (A, B) Volcano plot of metabolites from berries sampled the 29th day. Each point corresponds to a compounds within the same condition (A) or the same variety (B). The *x*-axis represents the $\log_2$ ratio CS/M (A) or HS/CTRL (B) of mean of relative quantity of each metabolite (mg/g of dry weight (DW)). The *y*-axis represents the $-\log_{10}$ *p*-value from Wilcoxon rank sum test. Labelled points corresponds to significant compounds different between varieties (A) or modulated by HS (B; *p*-value < 0.05 and $-0.1 > \log_2$ ratio > 0.1). (C) Quantity of each significant metabolite modulated by HS. Significant pair-wise comparison from Wilcoxon rank sum test between CTRL and HS within the same variety and between CS and M exposed to the same condition are indicated by *.

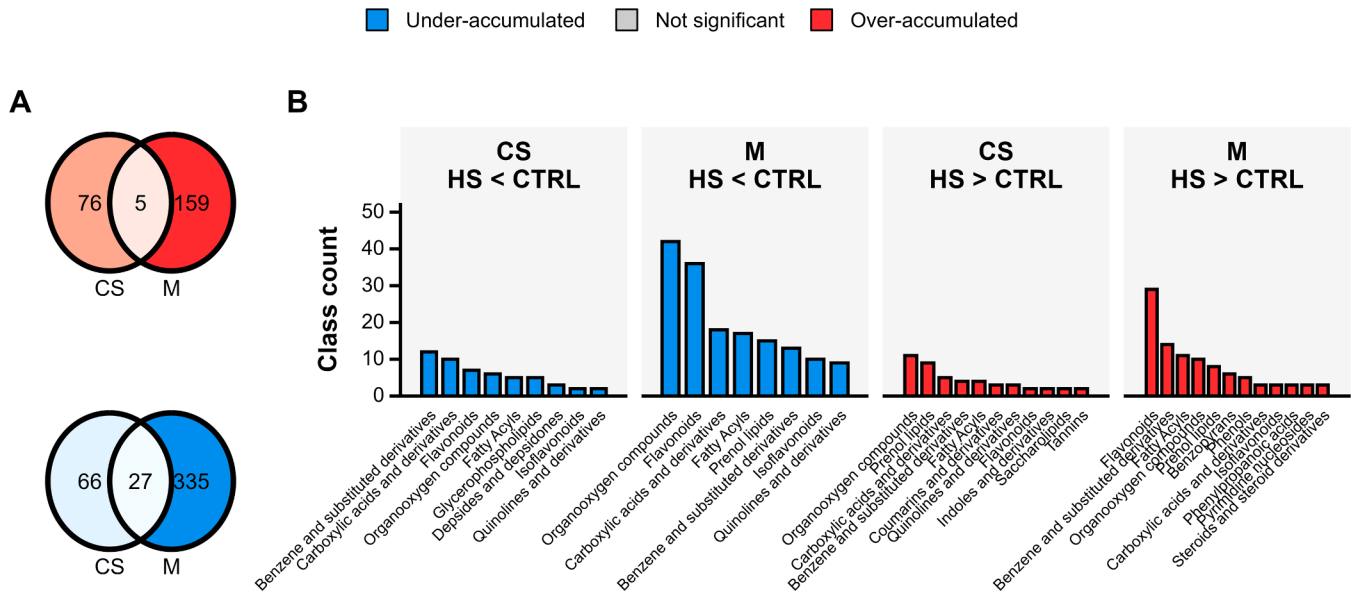

Fig. 8. Impact of heat stress (HS) compared to control (CTRL) on untargeted metabolites of Cabernet Sauvignon (CS) and Merlot (M) berries 23 days after 6-d HS. (A) Venn diagram of shared metabolites count between CS and M under- (left) or over-accumulated (right) following HS. (B) Frequency of top 8 represented classes of under- or over-accumulated metabolite following HS within each variety.

improve berry resistance against subsequent infection by *B. cinerea* only in CS (Fig. 3). Mycelial plug inoculation delivers a high infection pressure, similar to berry-to-berry mycelial spread, particularly in compact bunches, which is a key infection pathway. By assessing metabolites that inhibit this potent route, our approach provides a robust evaluation of berry resistance under controlled conditions. This result is in agreement with the well-known and often observed negative effects of leaf removal on *Botrytis* bunch rot, especially in Bordeaux vineyards (Hastoy et al., 2023; Pañitrur-De La Fuente et al., 2020). This practice is indeed more efficient when performed between bloom and veraison, *i.e.,* outside the major expression period of the disease, suggesting that early fruit developmental stages, such as the herbaceous berry stage studied herein, may be more responsive to such microclimate changes (Acimovic et al., 2016; Hed and Centinari, 2024; Molitor et al., 2011; Würz et al., 2020). Importantly, although all inoculations were performed under optimal conditions for disease establishment, the same HS treatment had no effect on M resistance, highlighting varietal specificities.

We further confirmed that the difference in susceptibility we observed was not due to an effect of HS on berry maturation, as our pathogen assays were conducted using CTRL- and HS-treated berries of equivalent maturity. Indeed, the dynamics of bunch ripening, monitored by the key mid-veraison stage, which reflects the accumulation *of* skin anthocyanins, were not significantly affected by HS or by variety (Fig. 4A). Although mid-veraison occurred later in 2023 than in 2024 for CS in the CTRL condition, mycelial progression was similar in both years, confirming that this maturity lag was too weak to influence the pathogenicity process. This absence of maturity delay was reinforced by a similar sugar accumulation (using TSS as proxy) regardless of the trial year, the applied temperature or the variety (Fig. 4B). While sugar concentration is a key parameter in the interactions with *B. cinerea*, organic acids such as malate and tartrate also influence susceptibility by limiting conidial cycling and serving as fungal substrates (Doneche and Pucheu-Plante, 1986). HS predominantly affects malic acid (Venios et al., 2020), with accelerated degradation observed with the same experimental set-up when HS occurred at veraison or ripening, whereas no significant effect on organic acids content was noted when HS was applied at the herbaceous stage (Lecourieux et al., 2017). Given the shorter stress period in our study, organic acid levels and pH were likely unchanged at inoculation. This is further supported by our targeted malate quantification at the time of inoculation, which revealed no significant differences between HS and CTRL berries, regardless of the cultivar (Supplemental Table 2). However, contrasting reports indicate that heat can transiently increase malate pre-veraison and accelerate its loss during ripening (Sweetman et al., 2014). Accordingly, it would be necessary to measure other maturity-related factor over a kinetics from the onset of 6-d HS to inoculation, such as berry skin toughness, to confirm that HS did not affect globally the maturity of the berries. Although classic HS markers have not been investigated (Pettenuzzo et al., 2022), the absence of any significant effect on the maturity parameters we measured suggests that the applied HS remained in a temperature range that grapevines are able to withstand without causing major impairment of key physiological functions (Venios et al., 2020). These results contrast with the delay in ripening caused by HS reported in other studies, particularly regarding anthocyanin accumulation (Dou et al., 2024; Mori et al., 2007; Movahed et al., 2016). However, in most of these studies, such discrepancies can be attributed to the application of HS to the whole plant and at more advanced maturity stages (veraison or ripening). Using the same setup on green bunches, Lecourieux et al. (2017) detected a delay in the onset of CS veraison following HS, as anthocyanins and sugars started to accumulate later but caught up to the same level as those in the CTRL at harvest. Given that the amplitude (+ 8 °C) and temperature reached (CTRL at ≃ 25 °C *vs.* HS at ≃ 35 °C) were similar in both experiments, the delay observed by Lecourieux et al. (2017) might be explained by the extended HS duration used (14 days, 12 h/day). This difference may also highlight a threshold effect according to heat duration, which could play a role in cluster ripening, therefore possibly modifying their subsequent susceptibility to *B. cinerea*. The use of a greenhouse equipped with a cooling system in the present study, allowing for a better control of the temperatures all along the experiment, might also stands for this discrepancy. Whatever the reason, HS also had no effect on berry growth or development in either variety, as assessed by measuring berry weight and volume (Fig. 4C, D), as already reported by Lecourieux et al. (2017).

A greater basal susceptibility to *B. cinerea* (CTRL) was demonstrated for CS than for M in our 2023 assay (Fig. 3), contrary to observations in vineyards (Pañitrur-De La Fuente et al., 2017). In vineyards, M is usually more susceptible than CS because it usually starts to ripen earlier. This results in earlier and greater fruit ontogenic susceptibility when gray mold epidemics are triggered at the same time during the growing

Table 5
Occurrence (> 50 %) and coefficient of variable from GLM performed on 2023 data of waxes, cutins monomers, targeted or untargeted metabolites variable, associated with mean of mycelial AUDPC.

Model	Variable	Occurrence	Coefficient	R^2	RMSE	CS/M		HS/CTRL	
						CTRL	HS	CS	M
Waxes	C30 alcohol	98	-35.3	0.7	134.99	-	-	ns	ns
	C28 aldehyde	98	59.01			+	ns	ns	ns
	α-Cyperene stereoisomer	93	42.34			ns	ns	ns	ns
	C22 alcohol	88	-26.47			ns	ns	ns	ns
	C32 aldehyde	79	21.32			+	+	ns	ns
	Uvaol	75	-14.55			-	-	ns	ns
	β-Sistosterol	68	22.73			ns	ns	ns	ns
	C20 fatty acid	67	-22.42			-	ns	ns	ns
	C32 alcohol	61	-31.34			ns	ns	ns	ns
	C26 ethyl ester fatty acid	61	-29.51			ns	ns	+	ns
	C23 alkane	55	24.33			ns	ns	ns	ns
	Oleanic acid / Ursolic acid	55	19.73			ns	ns	ns	ns
	C24 aldehyde	52	8.4			+	+	ns	ns
	γ-Tocopherol	50	17.92			ns	ns	ns	ns
Cutins	Coumaric acid	97	-46.2	0.72	122.32	ns	ns	ns	ns
	C16:0 dicarboxylic acid	93	-25.62			-	-	+	ns
	C18:2 ω-hydroxylated fatty acid	92	-26			-	-	+	+
	C18:1 dicarboxylic acid	89	-21.61			-	-	ns	ns
	C16:0 ω-hydroxylated fatty acid	87	-16.25			-	-	+	+
	C18:0 dihydroxylated fatty acid	77	-16.46			-	-	ns	ns
	Cinnamic acid	75	-21.49			ns	+	ns	ns
	C18:1 epoxylated ω-hydroxylated fatty acid	74	-13.42			-	-	ns	ns
Targeted	Catechin	97	-29.42	0.58	376.41	-	ns	ns	ns
	Proteins	96	34.23			ns	ns	ns	-
	Caffeic acid	95	35.3			ns	ns	ns	ns
	Cell wall	94	28.17			ns	ns	ns	ns
	trans-Coutaric acid	94	37.72			ns	+	ns	ns
	Glucose	91	-23.8			ns	ns	+	ns
	cis-Resveratrol	90	-21.69			-	-	ns	-
	ε-Viniferin isomer 1	82	-26.29			-	ns	ns	ns
	Hexose	72	-16.4			ns	ns	ns	ns
	cis-Coutaric acid	69	13.97			+	+	ns	ns
	Procyanidin B1	66	-12.13			ns	ns	ns	ns
	Epicatechin	65	-9.07			-	ns	ns	ns
	Amino acids	60	12.77			ns	+	-	-
	Isohopeaphenol	56	-8.69			-	ns	ns	ns
	Procyanidin isomer 2	55	-5.22			-	ns	ns	ns
	Epicatechin gallate	50	-6.06			-	ns	ns	ns
Untargeted	Pinocembrine	92	25.43	0.67	111.25	+	ns	-	ns
	Mono(2-ethyl-5-carboxypentyl) adipate	87	51.87			+	+	-	-
	Cyanidin-3,5-di-O-glucoside	78	40.91			+	+	-	ns
	D-Fructose 6-phosphate	73	-17.35			-	ns	+	-
	Unknown (9877)	72	14.97			+	ns	ns	ns
	2-Hydroxybenzonitrile	52	11.62			+	+	-	-

Each model R^2 abd RMSE are indicated. Positive and negative coefficient colored in red and blue, respectively. Significant (Wilcoxon rank sum test) positive (+) and negative (-) ratio (CS/M in CTRL or HS condition) and (HS/CTRL within CS or M variety) are indicated. ns: non-significant. Compounds with positive and negative coefficient associated with positive or negative CS/M ratio whatever the conditions, respectively, are linked to the varietal tolerance. Conversely, compounds with positive and negative coefficient associated with negative or positive HS/CTRL ratio within CS variety, respectively, are linked to HS induced tolerance. Ratio thus related to *B. cinerea* tolerance phenotype are indicated in green while those that are inconsistent with the GLM coefficient are indicated in grey.

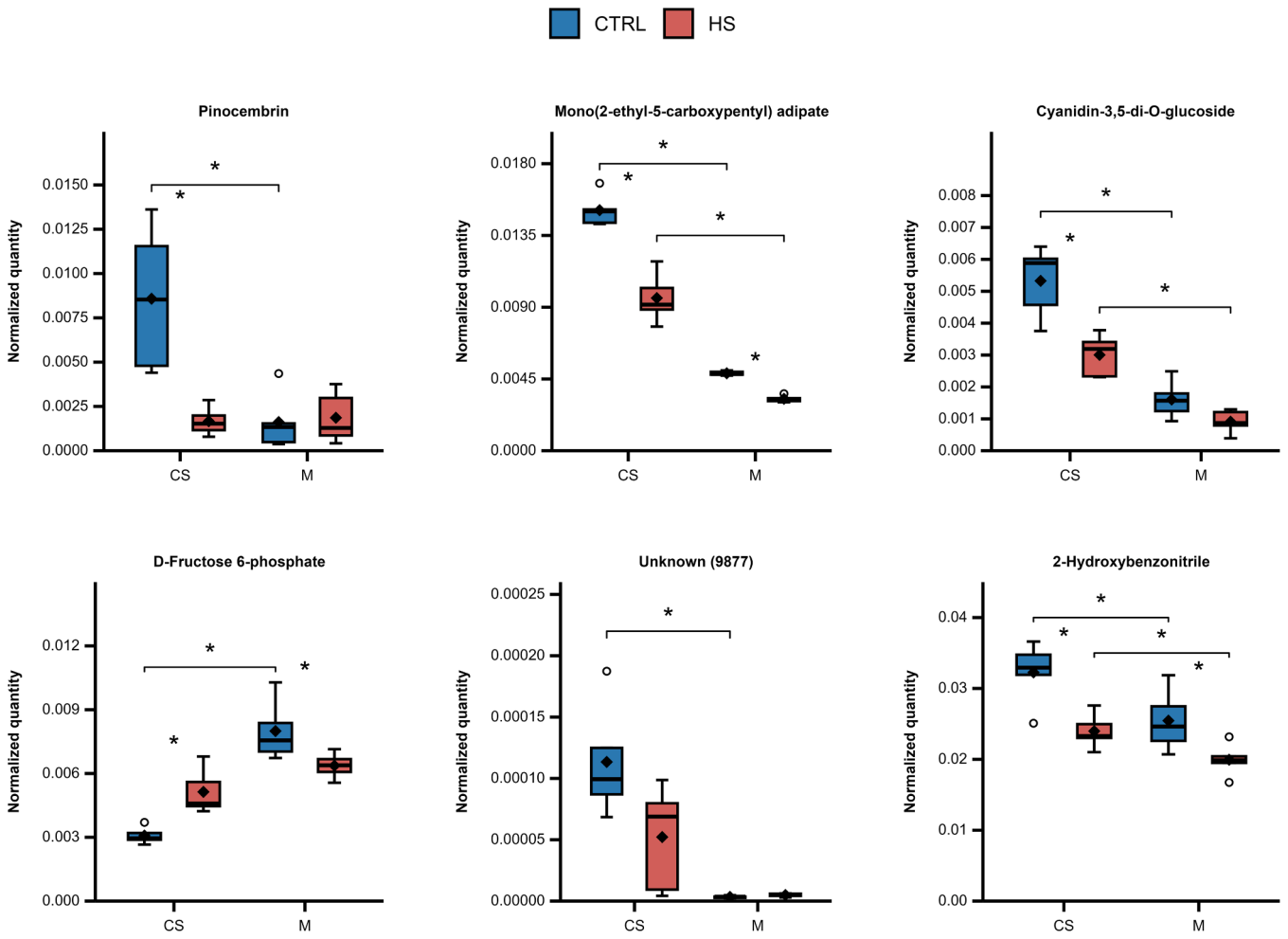

Fig. 9. Normalized quantity of untargeted metabolites from GLM analysis of Cabernet Sauvignon (CS) and Merlot (M) exposed to control (CTRL) and heat stress (HS). Compounds represented with an occurrence > 50 % from GLM analysis. Significant pair-wise comparison from Wilcoxon rank sum test between CTRL and HS within the same variety and between CS and M exposed to the same condition are indicated by *.

season (Deytieux-Belleau et al., 2009; Pañitrur-De La Fuente et al., 2017). Our study therefore took advantage of using fruiting cuttings with synchronized bunch ripening regardless of the cultivar, which allowed us to highlight varietal resistance independently of maturity. Despite the asynchrony fruit ripening within the bunch, the fine definition of the ripening stages at the berry level allowed us to verify and confirm that M berries had intrinsically greater resistance than CS in some equivalent developmental stages (Supplemental Figure 4).

Epicuticular waxes constitute the initial point of contact between *B. cinerea* and berries (Comménil et al., 1997), and they are involved in berry dehydration tolerance (VanderWeide et al., 2022). Surprisingly, the overall wax content was similar in the HS and CTRL berries of both cultivars 21 days after 6-d HS (Fig. 5A). In a similar study using three-year-old own-rooted Gewürztraminer, a 4-day HS applied in a growth chamber (CTRL at 20/30 °C *vs.* HS at 25/40 °C, n/d) either at middle ripening (single HS) or at veraison and middle ripening (double HS) triggered an overaccumulation of fatty acid and triterpenoid waxes and a reduction in fatty acyl esters at harvest (VanderWeide et al., 2022). Several parameters, such as a variety-dependent response, the different ripening stages subjected to HS, the temperatures reached and/or the exposure focused on bunches *vs.* whole plants, could explain this discrepancy.

In addition, the greater basal quantity of waxes found in the susceptible CS than in the resistant M in our study challenged their quantitative role as a physical barrier against the fungus. Several studies have revealed that waxes can promote susceptibility by helping pathogenic fungi to adhere, germinate or penetrate the host (Arya et al., 2021; Ziv et al., 2018). In table grapes, *B. cinerea* conidia germination was shown to be negatively and positively correlated with oleanolic acid and main primary alcohols (C22, C24 and C26) waxes, respectively (Silva-Moreno et al., 2016). In this study, CS and M presented similar contents of oleanic and ursolic acids, whereas C22, C24 and C26 primary alcohols were significantly more abundant in CS, which could correspond to more favorable conditions for the pathogen. On the host side, wax or cutin deficiency, which increases permeability, may lead to increased resistance in some cases. Faster diffusion of pathogen- or damage-associated molecular patterns (PAMPs and DAMPs, respectively) may, for example, lead to a quicker immune response and increased plant defenses before the fungus has become fully virulent (Arya et al., 2021; Ziv et al., 2018). Thus, the greater resistance of M, associated with a lower level of wax, could be caused by the impaired pathogenicity of *B. cinerea* and/or faster host defense induction, which remains to be tested.

Along the berry maturation process, epicuticular waxes form platelets that protrude with irregular patterns from the berry surface (Arand et al., 2021). The fruit surface becomes then porous, particularly with the increasing number of micro-cracks (Comménil et al., 1997; Gabler et al., 2003; Rogiers et al., 2005). The spraying of adjuvants disrupts and removes the platelets, which reduces the tolerance to *B. cinerea* (Rogiers et al., 2005). Thus, in association with their composition, the epicuticular waxes morphology also drives the interaction with *B. cinerea*. Therefore, a possible structural modification of epicuticular waxes by HS could have an impact on berry tolerance during fruit maturation. Fruit

post-harvest heat treatment is extensively used to improve shelf-life and attenuate decay caused by grey mould. For example, heat treatments of Citrus fruits were shown to prevent conidial germination by melting waxes structure and sealing skin micro-cracks (Schirra et al., 2000). Nevertheless, potential structural changes occurred following 6-d HS did not exclude a key role of abundant CS waxes in heat induced tolerance, not observed in M probably because of the lower wax amounts. Further studies using scanning electron micrographs should be carried out for investigating how HS may affect the structure of grape berry waxes.

More interestingly, our study revealed that the overaccumulation of cutin monomers (before inoculation) could be associated with increased CS resistance. Our 6-d HS clearly resulted in higher loads of C16:0 dicarboxylic acid, C18:2 ω-hydroxylated fatty acid and C16:0 ω-hydroxylated fatty acid (Fig. 5B, C). These results are original as cutin in grapevine berries is much less studied than waxes. In other host plants, several studies already reported a greater resistance to *B. cinerea* when somecuticle components, including cutin, overaccumulated (Arya et al., 2021; Ziv et al., 2018). Furthermore, in the present study, although statistically nonsignificant, the whole polymer amount tended to be slightly increased following the HS treatment, suggesting global reinforcement of the cutin layer. An increased amount of certain monomers could result in slower cutin polymer degradation by fungal cutinases and consequently increase resistance. The few characterized cutinases secreted by *B. cinerea* that have been well studied were all shown to efficiently degrade cutin (Liu et al., 2023; Salinas et al., 1986; van Kan et al., 1997). However, their activities did not correlate with strain aggressiveness (Salinas et al., 1986), and mutants were not impaired in pathogenicity, most likely because of the redundancy of these enzymes (Choquer et al., 2021; van Kan et al., 1997). With respect to the cultivar effect, all major cutin monomers were present in significantly greater quantities in M than in CS, which supports the quantitative role of cutin in greater resistance. Boulet et al. (2025) reported that the cutin monomer composition was slightly affected by the degree of berry maturation in Carignan and Grenache, but only two close maturity levels (± 1 % of potential alcohol, average of 12 %) were compared. In contrast, a marked decrease in the overall cutin content (by 2.5-fold) between fruit set and veraison increased Pinot Noir susceptibility at later stages, although cutin quantities did not differ between resistant and susceptible clones (Comménil et al., 1997). Interestingly, microscopic observations revealed that *B. cinerea* penetration pegs passed through only up to two-thirds of the cuticle thickness at the veraison stage (Kelloniemi et al., 2015), revealing a strong effect of the deeper layers of the cuticle on the resistance of young berries. Overall, our results highlighted the complex relationship between the quantitative cuticle composition and berry resistance against this pathogen. Transmission electron microscopy analyses could also be used to confirm the effect of HS on the thickness of the berry cuticle.

With respect to the whole-berry cell wall amount, our metabolite analysis revealed no clear differences regardless of the cultivar (Fig. 7A) or temperature treatment (Fig. 7B). Similarly, the whole-cell wall composition of complete berries was almost identical across ripening stages and between resistant and susceptible wine varieties (Weiller et al., 2021). However, by focusing on the skin of Pinot Noir (susceptible) and Chardonnay (resistant) berries, differences in cell wall composition and thickness have been related to varietal resistance (André et al., 2021). Similarly, the thickness and number of cell layers in the epidermis and external hypodermis have been correlated with a gradient of resistance in 42 table grape varieties (Gabler et al., 2003). Thus, considering the very low skin-to-pulp ratio (≃ 0.2; Bindon et al., 2011), our metabolomics analysis of whole berries may have missed important skin-specific cell wall modifications caused by HS. This assumption is supported by our previous omics experiments, which revealed that, in HS-treated CS berries, increased amounts of certain enzymes might contribute to cell wall expansion, loosening, and reinforcement *via* lignin synthesis (Lecourieux et al., 2020, 2017).

Stilbenic defenses in grape berries, including resveratrol and its polymers, are found in the exocarp, which is more abundant *ante* veraison, and their biosynthesis occurs mostly in the cell wall (Fornara et al., 2008). Although the present study examined the whole berry metabolome (excluding seeds), the stilbenes we identified most likely originated from berry skin. Several targeted stilbenes potentially fungitoxic against *B. cinerea* were found more abundant in M than in CS in the basal state (CTRL), and this higher fungitoxic load could be linked to the higher resistance of M against *B. cinerea*. After HS treatment, all the stilbenes diminished, but only cis-resveratrol and δ-viniferin remained more abundant in M than in CS, which nevertheless appeared sufficient to maintain greater resistance. Stilbene backbones are produced by stilbene synthases, a branching point of the phenylpropanoid pathway modulated by both biotic and abiotic stresses (Dubrovina and Kiselev, 2017). With a similar experimental design as that used herein, Lecourieux et al. (2017) highlighted that, in green bunches, the expression of some stilbene synthase genes was greater on the 1st and 7th days of HS but repressed after 14 days of HS. A poor correlation between transcript and protein accumulation was also noted (Lecourieux et al., 2020). This may explain why the quantity of stilbenes in CS berries remained unaffected by HS in our experiment. However, stilbene synthases in M were potentially repressed during the 6-d HS or recovery time, which would indicate a variety-dependent temperature sensitivity of these enzymes (or downstream enzymes). As one of the major fungitoxic stilbenes (monomers) in berries, resveratrol prevents *B. cinerea* conidial germination and hyphal growth (*in vitro* or sprayed on berries) by causing hyphal malformations and cell death (Adrian et al., 1997; Xu et al., 2018). The antifungal activity of stilbenes is highly correlated with their hydrophobicity, which increases their diffusion and permeabilization of the fungal cell membrane (Xu et al., 2018). Resveratrol induction *via* endogenous salicylic acid (following infection) or an exogenous functional analog (benzothiadiazole) was related to Marselan ontogenic and M-induced resistance against *B. cinerea* (Iriti et al., 2004; Kelloniemi et al., 2015). δ-viniferin is an endogenous oxidized derivative of resveratrol and is also produced by *B. cinerea* laccase through resveratrol dimerization (Cichewicz et al., 2000; Pezet et al., 2003a). Timperio et al. (2012) revealed the potential defensive role of δ-viniferins in leaves and flowers, with negligible levels for M (susceptible), whereas CS (resistant) contains a low constitutive amounts of it, with the content increasing following infection.

In the first step of *B. cinerea* infection, berry stilbenic defenses are enriched by *de novo* accumulation to reach a fungal toxicity threshold, but the speed of this response depends on the preformed stock (Jeandet et al., 1995; Kelloniemi et al., 2015; Montero et al., 2003). *B. cinerea* counterattacks by secreting laccases that specifically degrade stilbene compounds, allowing the fungus to be less exposed (Adrian et al., 1998; Pezet et al., 1991; Sbaghi et al., 1996). Fungal laccases also decrease the peak of induced stilbenes so that the total quantity is below the initial level in a few days (Montero et al., 2003). In addition, berries have the potential to slow the degradation of stilbenes with preformed tannins, which significantly and notably inhibit fungal laccases (Goetz et al., 1999; Perret et al., 2003; Vignault et al., 2020). Among their other protective roles, tannins are potential inhibitors of fungal pectinases, which reduces cell wall degradation (Porter and Schwartz, 1962; Scalbert, 1991). Thus, because the amount of condensed tannins (proanthocyanins) in grapevine fruit skin is positively correlated with berry ontogenic resistance to *B. cinerea* (Deytieux-Belleau et al., 2009), we consider of prime importance that both CS and M responded to HS through the overaccumulation of condensed tannins in the skin (Fig. 6). These tannins persisted until inoculation and therefore may account, at least in part, for the higher resistance of CS. As stilbenes, condensed tannins are localized in grapevine fruit skin (vacuole or cell wall), and apoplastic tannins exhibit a higher degree of polymerization, limiting their extractability (Gagné et al., 2006; Lecas and Brillouet, 1994). In a similar experiment with CS green bunches and 14 days of HS, many transcripts and corresponding enzymes within the flavonoid pathway were repressed, suggesting a decline in proanthocyanidin biosynthesis

and/or transport (Lecourieux et al., 2017, 2020). Thus, tannin overaccumulation in our experiment may have occurred, potentially, after the HS treatment, *i.e.,* during recovery. In an experiment where Shiraz bunches at the end of the berry set were subjected to a shorter but stronger HS (3 days; > 35 °C), the total tannin skin content was not affected when the HS was applied during the day, but the tannin galloylation level increased following the HS applied during day and night (Gouot et al., 2019). Similarly, higher temperatures at night (+8 °C) also increased proanthocyanin quantity and degree of polymerization at veraison and harvest in M berries (Cohen et al., 2008, 2012). Furthermore, our results are corroborated by the overaccumulation of skin condensed tannins following leaf removal in an M experimental vineyard near Bordeaux (Pañitrur-De La Fuente et al., 2020) further supporting the possible link between microclimate berry temperature, condensed tanins and resistance to Botrytis.

M berries displayed higher basal levels of defense-related metabolites such as cutin monomers, stilbenes, and flavan-3-ols compared to CS, which likely underlies their greater inherent resistance. Although HS reduced some fungitoxic compounds in M (*e.g.*, stilbenes and flavan-3-ols), the concomitant increase in tannins may compensate for this loss, maintaining resistance at levels similar to the control. The observed decline in flavan-3-ol monomers could reflect their incorporation into tannin polymers (Watrelot and Norton, 2020), though this remains to be confirmed. Notably, M resistance was not further enhanced beyond its basal level, possibly because susceptibility factors associated with berry maturity outweigh the effectiveness of these defenses at this developmental stage. Even after HS induction, the condensed tannin levels in M remained lower than those in CS, which suggests that a lower condensed tannin quantity associated with a higher stilbene quantity was sufficient to account for the M increased resistance against *B. cinerea*. Pezet et al. (2003b) reported that Gamaret is less susceptible than Gamay in part because the resistant variety accumulated more polymeric proanthocyanins during ripening, which maintained high inhibitory activity until and at maturity. Although more condensed tannins accumulated in CS than in M, the inhibitory activity of CS may be lower than that of M at the stage we studied. To verify this assumption, further investigations need to be performed to better understand the effect of HS and genotype on the precise composition and activity of tannins. In contrast, several flavan-3-ols were more abundant in our target analysis in M, notably in CTRL conditions. This contradictory result was possibly caused by the difficulty in extracting polymerized tannins complexed within cell walls (Gagné et al., 2006) and because the method we used for metabolomic analysis potentially targeted only vacuolar tannins.

Finaly, untargeted analysis coupled with GLM analysis revealed 6 candidates potentially involved in the HS-induced resistance of CS berries against *B. cinerea*. In 2023, the contrasting abundances of the two varieties and the two temperature conditions were highly related to mycelial progression. Although the identification remains to be confirmed, except for the unknown 9877 compound yet to be identified, their putative names potentially matched. D-Fructose-6-phosphate, in greater amounts in M berries, overaccumulated in heated CS berries. Sugar phosphate metabolism was repressed in heated CS berries (Lecourieux et al., 2017), which likely contributed to lower concentrations of sugar phosphate during HS (Lecourieux et al., 2020). These findings suggest that D-fructose-6-phosphate accumulated after HS treatment in the present study. Given its potential role as a scavenger of reactive oxygen species (Bogdanović et al., 2008), higher levels of D-fructose-6-phosphate in heated berries may contribute to maintaining cellular homeostasis under HS or during *B. cinerea* infection. However, the role of the 4 other susceptibility markers, namely, pinocembrin, mono(2-ethyl-5-carboxypentyl) adipate, cyanidin-3,5-di-O-glucoside, and 2-hydroxybenzonitrile, in the HS response and/or in *B. cinerea* resistance remains to be elucidated. Pinocembrin and cyanidin-3-O-glucoside are known antifungal flavonoids (Peng et al., 2012; Shain and Miller, 1982; Tao et al., 2010), which suggests that decreases in these flavonoids should not lead to increased resistance against *B. cinerea*. However, cyanidin-3-O-glucoside is degraded by *B. cinerea* laccases (Giménez et al., 2023), suggesting that cyanidin-3,5-di-O-glucoside could be detoxified by the fungus. In addition, cyanidin-3,5-di-O-glucoside is an antioxidant (Kumari et al., 2022) but was not related to the HS response in our study. In the literature, we found no information related to plant stress concerning mono (2-ethyl-5-carboxypentyl) adipate or 2-hydroxybenzonitrile.

Conclusion

Our study revealed that an increase (+10 °C HS for 6 days, 8 h/day) of the diurnal temperature, a key driver of the bunch microclimate, affected berry resistance against *B. cinerea*, even when the experimental heat wave occurred 3 weeks before inoculation. More specifically, CS berries at the herbaceous stage were responsive to HS, which increased their resistance, whereas M susceptibility against *B. cinerea* was unaffected despite significant metabolite changes. Since the higher susceptibility of the unheated CS CTRL berries was not related to an advanced maturity, it is highly probable that the modulation of preformed defenses and/or virulence-promoting factors by HS was partly responsible for disease reduction in the other scenario. In particular, our study clearly shows that the heat-induced resistance of CS berries was associated with an overaccumulation of skin defenses, especially specific cutin monomers and condensed tannins. In addition, untargeted metabolomics established a list of other potential candidates related to the CS response to HS and *de facto* likely linked to resistance against *B. cinerea*. The fact that M berries exhibited higher basal levels of several defense metabolites (*e.g.*, cutin monomers, stilbenes, and flavan-3-ols) compared to CS likely contributes to its greater basal resistance. Further investigations should consider the modifications of other known preformed constituents, notably skin cell walls, or of wax structural features, which may also play a key role in this interaction. Further experiments evaluating earlier and later inoculation points following the heat treatment are needed to assess the persistence and potential cultivar-dependence of heat-induced resistance against *B. cinerea*. In addition to the direct effect of the varietal genetic background and/or HS treatment on host preformed metabolites, a genotype-dependent response, such as a priming effect by HS, cannot be excluded. This could lead to differences in the amplitude and speed of the host immune response. The assessment of the accumulation of stilbenic phytoalexins and/or pathogenesis-related proteins during the course of infection could also be helpful for further understanding disease outcomes.

CRediT authorship contribution statement

Erwan Chavonet: Writing – review & editing, Writing – original draft, Visualization, Validation, Software, Methodology, Investigation, Formal analysis, Conceptualization. **Cathleen Mirande-Ney:** Writing – review & editing, Visualization, Software, Methodology, Investigation, Formal analysis, Conceptualization. **Sarah Bernardo:** Validation, Investigation. **Clément Guinand:** Validation, Investigation. **Ghislain Delestre:** Validation, Investigation. **Xi Zhan:** Validation, Resources. **Josep Valls Fonayet:** Validation, Investigation. **Sylvain Prigent:** Software. **Pierre Van Delft:** Resources. **Stéphanie Pascal:** Validation, Investigation. **Jérôme Joubès:** Writing – review & editing, Supervision, Methodology, Conceptualization. **David Lecourieux:** Writing – review & editing, Supervision, Methodology, Formal analysis, Conceptualization. **Marc Fermaud:** Writing – review & editing, Supervision, Methodology, Formal analysis, Conceptualization. **Frédéric Domergue:** Writing – review & editing, Supervision, Project administration, Methodology, Investigation, Formal analysis, Conceptualization.

Declaration of competing interest

The authors declare that they have no known competing financial interests or personal relationships that could have appeared to influence

the work reported in this paper.

Acknowledgments

This study received financial support from the French government in the framework of the IdEX Bordeaux University “Investments for the Future” program / GPR Bordeaux Plant Sciences. Authors thank Bordeaux-Metabolome platform for lipid analysis (https://www.biomemb.cnrs.fr/en/lipidomic-plateform/) supported by the MetaboHUB infrastructure funded by the Agence Nationale de la Recherche under the France 2030 program (MetaboHUB ANR-11-INBS-0010; MetEx+ ANR-21-ESRE-0035; MetaboHUB (JVCE) ANR-24-INBS-0012). Authors acknowledge the Bordeaux INRAE – BSA - IFV Mixt Technology Unit « UMT SEVEN ». Authors are also gratefull to the authors services of Springer Nature for their participation to the edition of the manuscript for proper English language, grammar, punctuation, spelling, and overall style (SNAS verification code 6927-D6EF-B7CC-3F44-9130). Authors finaly thank Eric Duffau, Thomas Lopez and Alexandra Besse for their helpful contribution in preparing experimental set-up and samples during their internships, as well as Claire Bréhélin for participating in symptoms notation. Special thanks to Jean-Pierre Petit for preparing 2023 fruiting cuttings and his priceless training for the 2024 and future productions.

Supplementary materials

Supplementary material associated with this article can be found, in the online version, at doi:10.1016/j.stress.2025.101051.

Data availability

Data will be made available on request.

References

Acimovic, D., Tozzini, L., Green, A., Sivilotti, P., Sabbatini, P., 2016. Identification of a defoliation severity threshold for changing fruitset, bunch morphology and fruit composition in Pinot Noir. Aust. J. Grape Wine Res. 22, 399–408. https://doi.org/10.1111/ajgw.12235.

Adrian, M., Jeandet, P., Veneau, J., Weston, L.A., Bessis, R., 1997. Biological activity of resveratrol, a stilbenic compound from grapevines, against *Botrytis cinerea*, the causal agent for gray mold. J. Chem. Ecol. 23, 1689–1702. https://doi.org/10.1023/B:JOEC.0000006444.79951.75.

Adrian, M., Rajaei, H., Jeandet, P., Veneau, J., Bessis, R., 1998. Resveratrol oxidation in *Botrytis cinerea* conidia. Phytopathology 88, 472–476. https://doi.org/10.1094/PHYTO.1998.88.5.472.

Agbangba, C.E., Aide, E.S., Honfo, H., Kakai, R.G., 2024. On the use of post-hoc tests in environmental and biological sciences: a critical review. Heliyon 10. https://doi.org/10.1016/j.heliyon.2024.e25131.

Ahlmann-Eltze, C., Patil, I., 2022. ggsignif: significance brackets for “ggplot2.”.

Ahlmann-Eltze, C., Patil, I., 2021. ggsignif: r package for displaying significance brackets for “ggplot2.” https://doi.org/10.31234/osf.io/7awm6.

André, M., Lacampagne, S., Barsacq, A., Gontier, E., Petrel, M., Mercier, L., Courot, D., Gény-Denis, L., 2021. Physical, anatomical, and biochemical composition of skins cell walls from two grapevine cultivars (*Vitis vinifera*) of Champagne region related to their susceptibility to *Botrytis cinerea* during ripening. Horticulturae 7, 413. https://doi.org/10.3390/horticulturae7100413.

Arand, K., Bieler, E., Dürrenberger, M., Kassemeyer, H.-H., 2021. Developmental pattern of grapevine (*Vitis vinifera* L.) berry cuticular wax: differentiation between epicuticular crystals and underlying wax. PLoS One 16, e0246693. https://doi.org/10.1371/journal.pone.0246693.

Arya, G.C., Sarkar, S., Manasherova, E., Aharoni, A., Cohen, H., 2021. The plant cuticle: an ancient guardian barrier set against long-standing rivals. Front. Plant. Sci. 12, 663165.

Auguie, B., Antonov, A., 2017. gridExtra: miscellaneous functions for “grid” graphics.

Bindon, K., Myburgh, P., Oberholster, A., Roux, K., Toit, C.du, 2011. Response of grape and wine phenolic composition in *vitis vinifera* L. cv. Merlot to variation in grapevine water status. SAJEV 32, 71–88. https://doi.org/10.21548/32-1-1368.

Blanco-Ulate, B., Labavitch, J.M., Vincenti, E., Powell, A.L.T., Cantu, D., 2016. Hitting the wall: plant cell walls during *Botrytis cinerea* infections. In: Fillinger, S., Elad, Y. (Eds.), Botrytis – The Fungus, the Pathogen and Its Management in Agricultural Systems. Springer International Publishing, Cham, pp. 361–386. https://doi.org/10.1007/978-3-319-23371-0_18.

Blanco-Ulate, B., Morales-Cruz, A., Amrine, K.C.H., Labavitch, J.M., Powell, A.L.T., Cantu, D., 2014. Genome-wide transcriptional profiling of *Botrytis cinerea* genes targeting plant cell walls during infections of different hosts. Front. Plant Sci. 5. https://doi.org/10.3389/fpls.2014.00435.

Bogdanović, J., Mojović, M., Milosavić, N., Mitrović, A., Vučinić, Ž., Spasojević, I., 2008. Role of fructose in the adaptation of plants to cold-induced oxidative stress. Eur. Biophys. J. 37, 1241–1246. https://doi.org/10.1007/s00249-008-0260-9.

Boulet, J.-C., Meudec, E., Ducasse, M.-A., Abi-Habib, E., Gall, S.L., Falourd, X., Bakan, B., Traore, A., Lucchi, G., Gourrat, K., Peltier, C., Poncet-Legrand, C., Vernhet, A., Cheynier, V., 2025. Insights into multiscale chemical characterisation for the understanding of berry maturation. OENO One 59. https://doi.org/10.20870/oeno-one.2025.59.1.8286.

Bourdenx, B., Bernard, A., Domergue, F., Pascal, S., Léger, A., Roby, D., Pervent, M., Vile, D., Haslam, R.P., Napier, J.A., Lessire, R., Joubès, J., 2011. Overexpression of Arabidopsis ECERIFERUM1 promotes wax very-long-chain alkane biosynthesis and influences plant response to biotic and abiotic stresses. Plant Physiol. 156, 29–45. https://doi.org/10.1104/pp.111.172320.

Bradford, M.M., 1976. A rapid and sensitive method for the quantitation of microgram quantities of protein utilizing the principle of protein-dye binding. Anal. Biochem. 72, 248–254. https://doi.org/10.1016/0003-2697(76)90527-3.

Broome, J.C., English, J.T., Marois, J.J., Latorre, B.A., Aviles, J.C., 1995. Development of an infection model for Botrytis bunch rot of grapes based on wetness duration and temperature. Phytopathology 85, 97. https://doi.org/10.1094/Phyto-85-97.

Calvo-Garrido, C., Viñas, I., Elmer, P.A., Usall, J., Teixidó, N., 2014. Suppression of *Botrytis cinerea* on necrotic grapevine tissues by early-season applications of natural products and biological control agents. Pest Manag. Sci. 70, 595–602. https://doi.org/10.1002/ps.3587.

Cameron, A., Brand, T. van den, 2025. geomtextpath: curved text in “ggplot2.”.

Carvalho, L.C., Coito, J.L., Colaço, S., Sangiogo, M., Amâncio, S., 2015. Heat stress in grapevine: the pros and cons of acclimation. Plant Cell Environ. 38, 777–789. https://doi.org/10.1111/pce.12445.

Chang, W., 2023. Extrafont: tools for using fonts.

Choquer, M., Rascle, C., Gonçalves, I.R., de Vallée, A., Ribot, C., Loisel, E., Smilevski, P., Ferria, J., Savadogo, M., Souibgui, E., Gagey, M.-J., Dupuy, J.-W., Rollins, J.A., Marcato, R., Noûs, C., Bruel, C., Poussereau, N., 2021. The infection cushion of *Botrytis cinerea*: a fungal ‘weapon’ of plant-biomass destruction. Environ. Microbiol. 23, 2293–2314. https://doi.org/10.1111/1462-2920.15416.

Cichewicz, R.H., Kouzi, S.A., Hamann, M.T., 2000. Dimerization of resveratrol by the grapevine pathogen *Botrytis cinerea*. J. Nat. Prod. 63, 29–33. https://doi.org/10.1021/np990266n.

Cohen, S.D., Tarara, J.M., Gambetta, G.A., Matthews, M.A., Kennedy, J.A., 2012. Impact of diurnal temperature variation on grape berry development, proanthocyanidin accumulation, and the expression of flavonoid pathway genes. J. Exp. Bot. 63, 2655–2665. https://doi.org/10.1093/jxb/err449.

Cohen, S.D., Tarara, J.M., Kennedy, J.A., 2008. Assessing the impact of temperature on grape phenolic metabolism. Anal. Chim. Acta 621, 57–67. https://doi.org/10.1016/j.aca.2007.11.029. Papers presented at the 5th Symposium In Vino Analytica Scientia.

Comménil, P., Belingheri, L., Bauw, G., Dehorter, B., 1999. Molecular characterization of a lipase induced in *Botrytis cinerea* by components of grape berry cuticle. Physiol. Mol. Plant Pathol. 55, 37–43. https://doi.org/10.1006/pmpp.1999.0206.

Comménil, P., Brunet, L., Audran, J.-C., 1997. The development of the grape berry cuticle in relation to susceptibility to bunch rot disease. J. Exp. Bot. 48, 1599–1607. https://doi.org/10.1093/jxb/48.8.1599.

Dai, Z.W., Meddar, M., Renaud, C., Merlin, I., Hilbert, G., Delrot, S., Gomès, E., 2014. Long-term *in vitro* culture of grape berries and its application to assess the effects of sugar supply on anthocyanin accumulation. J. Exp. Bot. 65, 4665–4677. https://doi.org/10.1093/jxb/ert489.

de Mendiburu, F., 2023. agricolae: statistical procedures for agricultural research.

Deytieux-Belleau, C., Geny, L., Roudet, J., Mayet, V., Donèche, B., Fermaud, M., 2009. Grape berry skin features related to ontogenic resistance to *Botrytis cinerea*. Eur. J. Plant Pathol. 125, 551–563. https://doi.org/10.1007/s10658-009-9503-6.

Djoumbou Feunang, Y., Eisner, R., Knox, C., Chepelev, L., Hastings, J., Owen, G., Fahy, E., Steinbeck, C., Subramanian, S., Bolton, E., Greiner, R., Wishart, D.S., 2016. ClassyFire: automated chemical classification with a comprehensive, computable taxonomy. J. Cheminform. 8, 61. https://doi.org/10.1186/s13321-016-0174-y.

Domergue, F., Vishwanath, S.J., Joubès, J., Ono, J., Lee, J.A., Bourdon, M., Alhattab, R., Lowe, C., Pascal, S., Lessire, R., Rowland, O., 2010. Three Arabidopsis fatty acyl-coenzyme A reductases, FAR1, FAR4, and FAR5, generate primary fatty alcohols associated with suberin deposition. Plant Physiol. 153, 1539–1554. https://doi.org/10.1104/pp.110.158238.

Doneche, B., Pucheu-Plante, B., 1986. Influence of various parameters upon the growth of *Botrytis cinerea* on synthetic medium: definition of a conidian cycle. Vitis 25, 21–30.

Dou, F., Phillip, F.O., Liu, H., 2024. Combined metabolome and transcriptome analysis revealed the accumulation of anthocyanins in grape berry (*Vitis vinifera* L.) under high-temperature stress. Plants 13, 2394. https://doi.org/10.3390/plants13172394.

Dubrovina, A.S., Kiselev, K.V., 2017. Regulation of stilbene biosynthesis in plants. Planta 246, 597–623. https://doi.org/10.1007/s00425-017-2730-8.

Elmer, P.A.G., Michailides, T.J., 2007. Epidemiology of *Botrytis cinerea* in orchard and vine crops. In: Elad, Y., Williamson, B., Tudzynski, P., Delen, N. (Eds.), Botrytis: Biology, Pathology and Control. Springer Netherlands, Dordrecht, pp. 243–272. https://doi.org/10.1007/978-1-4020-2626-3_14.

Evans, K.J., Pirie, A.J.G., 2024. Weather variables for within-vineyard awareness of botrytis risk. Aust. J. Grape Wine Res. 2024, 6630039. https://doi.org/10.1155/2024/6630039.

FC, M., Davis, T.L., 2024. ggpattern: “ggplot2” pattern geoms.

Fedele, G., González-Domínguez, E., Delière, L., Díez-Navajas, A.M., Rossi, V., 2020. Consideration of latent infections improves the prediction of botrytis bunch rot severity in vineyards. Plant Dis. 104, 1291–1297. https://doi.org/10.1094/PDIS-11-19-2309-RE.

Fernández, V., Guzmán-Delgado, P., Graça, J., Santos, S., Gil, L., 2016. Cuticle structure in relation to chemical composition: re-assessing the prevailing model. Front. Plant Sci. 7, 427.

Fornara, V., Onelli, E., Sparvoli, F., Rossoni, M., Aina, R., Marino, G., Citterio, S., 2008. Localization of stilbene synthase in *Vitis vinifera* L. during berry development. Protoplasma 233, 83–93. https://doi.org/10.1007/s00709-008-0309-8.

Fox, J., Weisberg, S., 2018. An R companion to Applied Regression. SAGE, Thousand Oaks CA.

Fox, J., Weisberg, S., Price, B., Adler, D., Bates, D., Baud-Bovy, G., Bolker, B., Ellison, S., Firth, D., Friendly, M., Gorjanc, G., Graves, S., Heiberger, R., Krivitsky, P., Laboissiere, R., Maechler, M., Monette, G., Murdoch, D., Nilsson, H., Ogle, D., Ripley, B., Short, T., Venables, W., Walker, S., Winsemius, D., Zeileis, A., R-Core, 2024. CAR: companion to applied regression.

Friedman, J.H., Hastie, T., Tibshirani, R., 2010. Regularization paths for generalized linear models via coordinate descent. J. Stat. Softw. 33, 1–22. https://doi.org/10.18637/jss.v033.i01.

Gabler, F.M., Smilanick, J.L., Mansour, M., Ramming, D.W., Mackey, B.E., 2003. Correlations of morphological, anatomical, and chemical features of grape berries with resistance to *Botrytis cinerea*. Phytopathology 93, 1263–1273. https://doi.org/10.1094/PHYTO.2003.93.10.1263.

Gagné, S., Saucier, C., Gény, L., 2006. Composition and cellular localization of tannins in Cabernet Sauvignon skins during growth. J. Agric. Food Chem. 54, 9465–9471. https://doi.org/10.1021/jf061946g.

Gambetta, G.A., Kurtural, S.K., 2021. Global warming and wine quality: are we close to the tipping point? OENO One 55, 353–361. https://doi.org/10.20870/oeno-one.2021.55.3.4774.

Gao, C.-H., Yu, G., Dusa, A., Akyol, T.Y., 2024. ggVennDiagram: a "ggplot2" implement of Venn diagram.

Geny, L., Ollat, N., Soyer, J.-P., 1998. Grapevine fruiting cuttings: validation of an experimental system to study grapevine physiology. II. Study of grape development. OENO One 32, 83–90. https://doi.org/10.20870/oeno-one.1998.32.2.1052.

Ghiglieno, I., Mattivi, F., Cola, G., Trionfini, D., Perenzoni, D., Simonetto, A., Gilioli, G., Valenti, L., 2020. The effects of leaf removal and artificial shading on the composition of Chardonnay and Pinot noir grapes. OENO One 54, 761–777. https://doi.org/10.20870/oeno-one.2020.54.4.2556.

Giménez, P., Just-Borràs, A., Gombau, J., Canals, J.M., Zamora, F., 2023. Effects of laccase from *Botrytis cinerea* on the oxidative degradation of anthocyanins. OENO One 57, 243–253. https://doi.org/10.20870/oeno-one.2023.57.3.7567.

Goetz, G., Fkyerat, A., Métais, N., Kunz, M., Tabacchi, R., Pezet, R., Pont, V., 1999. Resistance factors to grey mould in grape berries: identification of some phenolics inhibitors of *botrytis cinerea* stilbene oxidase. Phytochemistry 52, 759–767. https://doi.org/10.1016/S0031-9422(99)00351-9.

González, C., Brito, N., Sharon, A., 2016. Infection process and fungal virulence factors. In: Fillinger, S., Elad, Y. (Eds.), Botrytis – The Fungus, the Pathogen and Its Management in Agricultural Systems. Springer International Publishing, Cham, pp. 229–246. https://doi.org/10.1007/978-3-319-23371-0_12.

Gorshkov, V., Tsers, I., 2022. Plant susceptible responses: the underestimated side of plant–pathogen interactions. Biol. Rev. 97, 45–66. https://doi.org/10.1111/brv.12789.

Gouot, J.C., Smith, J.P., Holzapfel, B.P., Barril, C., 2019. Impact of short temperature exposure of *Vitis vinifera* L. cv. Shiraz grapevine bunches on berry development, primary metabolism and tannin accumulation. Environ. Exp. Bot. 168, 103866. https://doi.org/10.1016/j.envexpbot.2019.103866.

Graves, S., Piepho, H.-P., Selzer, L., Dorai-Raj, S., 2024. multcompView: visualizations of paired comparisons.

Hastoy, X., Franc, C., Riquier, L., Ségur, M.-C., Revel, G.D., Fermaud, M., 2023. Fungitoxic role of endogenous eugenol in the hybrid grapevine cultivar Baco blanc resistant to *Botrytis cinerea*. OENO One 57, 159–175. https://doi.org/10.20870/oeno-one.2023.57.2.7454.

Hed, B., Centinari, M., 2024. Mechanical leaf removal for improved Botrytis bunch rot control in *Vitis vinifera* 'Pinot gris' and 'Pinot noir' grapevines in the northeastern United States. Plant Dis. 108, 3156–3162. https://doi.org/10.1094/PDIS-02-24-0383-RE.

Hed, B., Ngugi, H.K., Travis, J.W., 2009. Relationship between cluster compactness and bunch rot in vignoles grapes. Plant Dis. 93, 1195–1201. https://doi.org/10.1094/PDIS-93-11-1195.

Herzog, K., Schwander, F., Kassemeyer, H.-H., Bieler, E., Dürrenberger, M., Trapp, O., Töpfer, R., 2022. Towards sensor-based phenotyping of physical barriers of grapes to improve resilience to Botrytis bunch rot. Front. Plant Sci. 12, 808365. https://doi.org/10.3389/fpls.2021.808365.

Hewitt, S., Hernández-Montes, E., Dhingra, A., Keller, M., 2023. Impact of heat stress, water stress, and their combined effects on the metabolism and transcriptome of grape berries. Sci. Rep. 13, 9907. https://doi.org/10.1038/s41598-023-36160-x.

Hugh-Jones, D., 2024. ggmagnify: create a magnified inset of part of a "ggplot" object.

Iriti, M., Rossoni, M., Borgo, M., Faoro, F., 2004. Benzothiadiazole enhances resveratrol and anthocyanin biosynthesis in grapevine, meanwhile improving resistance to *Botrytis cinerea*. J. Agric. Food Chem. 52, 4406–4413. https://doi.org/10.1021/jf049487b.

Jeandet, P., Bessis, R., Sbaghi, M., Meunier, P., 1995. Production of the Phytoalexin Resveratrol by grapes as a response to *Botrytis* attack under natural conditions. J. Phytopathol. 143, 135–139. https://doi.org/10.1111/j.1439-0434.1995.tb00246.x.

Kassambara, A., 2023. ggpubr: "ggplot2" based publication ready plots.

Kay, M., 2024. ggdist: visualizations of distributions and uncertainty in the grammar of graphics. IEEE Trans. Vis. Comput. Graph. 30, 414–424. https://doi.org/10.1109/TVCG.2023.3327195.

Kay, M., Wiernik, B.M., 2024. ggdist: visualizations of distributions and uncertainty.

Kelloniemi, J., Trouvelot, S., Héloir, M.-C., Simon, A., Dalmais, B., Frettinger, P., Cimerman, A., Fermaud, M., Roudet, J., Baulande, S., Bruel, C., Choquer, M., Couvelard, L., Duthieuw, M., Ferrarini, A., Flors, V., Le Pèchеur, P., Loisel, E., Morgant, G., Poussereau, N., Pradier, J.-M., Rascle, C., Trdá, L., Poinssot, B., Viaud, M., 2015. Analysis of the molecular dialogue between gray mold (*Botrytis cinerea*) and grapevine (*Vitis vinifera*) reveals a clear shift in defense mechanisms during berry ripening. MPMI 28, 1167–1180. https://doi.org/10.1094/MPMI-02-15-0039-R.

Kozak, M., Piepho, H.-P., 2018. What's normal anyway? Residual plots are more telling than significance tests when checking ANOVA assumptions. J. Agron. Crop Sci. 204, 86–98. https://doi.org/10.1111/jac.12220.

Kretschmer, M., Kassemeyer, H.-H., Hahn, M., 2007. Age-dependent grey mould susceptibility and tissue-specific defence gene activation of grapevine berry skins after infection by *Botrytis cinerea*. J. Phytopathol. 155, 258–263. https://doi.org/10.1111/j.1439-0434.2007.01216.x.

Krzywinski, M., Altman, N., 2014. Nonparametric tests. Nat. Methods 11, 467–468. https://doi.org/10.1038/nmeth.2937.

Kumari, P., Raju, D.V.S., Prasad, K.V., Saha, S., Panwar, S., Paul, S., Banyal, N., Bains, A., Chawla, P., Fogarasi, M., Fogarasi, S., 2022. Characterization of anthocyanins and their antioxidant activities in indian rose varieties (*Rosa* × *hybrida*) using HPLC. Antioxidants 11, 2032. https://doi.org/10.3390/antiox11102032.

Lecas, M., Brillouet, J.-M., 1994. Cell wall composition of grape berry skins. Phytochemistry 35, 1241–1243. https://doi.org/10.1016/S0031-9422(00)94828-3.

Lecourieux, D., Kappel, C., Claverol, S., Pieri, P., Feil, R., Lunn, J.E., Bonneu, M., Wang, L., Gomès, E., Delrot, S., Lecourieux, F., 2020. Proteomic and metabolomic profiling underlines the stage- and time-dependent effects of high temperature on grape berry metabolism. J. Integr. Plant Biol. 62, 1132–1158. https://doi.org/10.1111/jipb.12894.

Lecourieux, F., Kappel, C., Pieri, P., Charon, J., Pillet, J., Hilbert, G., Renaud, C., Gomès, E., Delrot, S., Lecourieux, D., 2017. Dissecting the biochemical and transcriptomic effects of a locally applied heat treatment on developing Cabernet Sauvignon grape berries. Front. Plant Sci. 8, 53. https://doi.org/10.3389/fpls.2017.00053.

Liu, M., Zong, Z., Fang, X., Liu, R., Mu, H., Chen, H., Niu, B., Gao, H., 2023. Purification and characterization of cutinase from *Botrytis cinerea* and effect on blueberry cuticle. J. Agric. Food Res. 12, 100599. https://doi.org/10.1016/j.jafr.2023.100599.

Luna, E., Flandin, A., Cassan, C., Prigent, S., Chevanne, C., Kadiri, C.F., Gibon, Y., Pétriacq, P., 2020. Metabolomics to exploit the primed immune system of tomato fruit. Metabolites 10, 96. https://doi.org/10.3390/metabo10030096.

Mangiafico, S., 2024. rcompanion: functions to support extension education program evaluation.

Martinez, F., Blancard, D., Lecomte, P., Levis, C., Dubos, B., Fermaud, M., 2003. Phenotypic differences between vacuma and transposa subpopulations of *Botrytis cinerea*. Eur. J. Plant Pathol. 109, 479–488. https://doi.org/10.1023/A:1024222206991.

Moerschbacher, B., Mendgen, K., 2000. Structural aspects of defense. In: Slusarenko, A. J., Fraser, R.S.S., van Loon, L.C. (Eds.), Mechanisms of Resistance to Plant Diseases. Springer Netherlands, Dordrecht, pp. 231–277. https://doi.org/10.1007/978-94-011-3937-3_8.

Molitor, D., Behr, M., Fischer, S., Hoffmann, L., Evers, D., 2011. Timing of cluster-zone leaf removal and its impact on canopy morphology, cluster structure and bunch rot susceptibility of grapes. OENO One 45, 149–159. https://doi.org/10.20870/oeno-one.2011.45.3.1495.

Molitor, D., Behr, M., Hoffmann, L., Evers, D., 2012. Impact of grape cluster division on cluster morphology and bunch rot epidemic. Am. J. Enol. Vitic. 63, 508–514. https://doi.org/10.5344/ajev.2012.12041.

Montero, C., Cristescu, S.M., Jiménez, J.B., Orea, J.M., te Lintel Hekkert, S., Harren, F.J. M., González Ureña, A., 2003. Trans-resveratrol and grape disease resistance. A dynamical study by high-resolution laser-based techniques. Plant Physiol. 131, 129–138. https://doi.org/10.1104/pp.010074.

Mori, K., Goto-Yamamoto, N., Kitayama, M., Hashizume, K., 2007. Loss of anthocyanins in red-wine grape under high temperature. J. Exp. Bot. 58, 1935–1945. https://doi.org/10.1093/jxb/erm055.

Movahed, N., Pastore, C., Cellini, A., Allegro, G., Valentini, G., Zenoni, S., Cavallini, E., D'Incà, E., Tornielli, G.B., Filippetti, I., 2016. The grapevine *VviPrx31* peroxidase as a candidate gene involved in anthocyanin degradation in ripening berries under high temperature. J. Plant Res. 129, 513–526. https://doi.org/10.1007/s10265-016-0786-3.

Müller, T., Bronkhorst, J., Müller, J., Safari, N., Hahn, M., Sprakel, J., Scheuring, D., 2024. Plant infection by the necrotrophic fungus Botrytis requires actin-dependent generation of high invasive turgor pressure. New Phytol. 244, 192–201. https://doi.org/10.1111/nph.20025.

Ogle, D.H., Doll, J.C., Wheeler, A.P., Dinno, A., 2025. FSA: simple fisheries stock assessment methods.

Ollat, N., Geny, L., Soyer, J.-P., 1998. Grapevine fruiting cuttings: validation of an experimental system to study grapevine physiology. I. Main vegetative characteristics. OENO One 32, 1–9. https://doi.org/10.20870/oeno-one.1998.32.1.1061.

Osbourn, A.E., 1996. Preformed antimicrobial compounds and plant defense against fungal attack. Plant Cell 8, 1821–1831. https://doi.org/10.1105/tpc.8.10.1821.

Pañitrur-De La Fuente, C., Valdés-Gómez, H., Roudet, J., Acevedo-Opazo, C., Verdugo-Vásquez, N., Araya-Alman, M., Lolas, M., Moreno, Y., Fermaud, M., 2017. Classification of winegrape cultivars in Chile and France according to their susceptibility to *Botrytis cinerea* related to fruit maturity. Aust. J. Grape Wine Res. 24, 145–157. https://doi.org/10.1111/ajgw.12315.

Pañitrur-De La Fuente, C., Valdés-Gómez, H., Roudet, J., Verdugo-Vásquez, N., Mirabal, Y., Laurie, V.F., Goutouly, J.P., Opazo, C.A., Fermaud, M., 2020. Vigor thresholded NDVI is a key early risk indicator of Botrytis bunch rot in vineyards. OENO One 54, 279–297. https://doi.org/10.20870/oeno-one.2020.54.2.2954.

Peng, L., Yang, S., Cheng, Y.J., Chen, F., Pan, S., Fan, G., 2012. Antifungal activity and action mode of pinocembrin from propolis against *Penicillium italicum*. Food Sci. Biotechnol. 21, 1533–1539. https://doi.org/10.1007/s10068-012-0204-0.

Pensec, F., Pączkowski, C., Grabarczyk, M., Woźniak, A., Bénard-Gellon, M., Bertsch, C., Chong, J., Szakiel, A., 2014. Changes in the triterpenoid content of cuticular waxes during fruit ripening of eight grape (*Vitis vinifera*) cultivars grown in the upper rhine valley. J. Agric. Food Chem. 62, 7998–8007. https://doi.org/10.1021/jf502033s.

Perret, C., Pezet, R., Tabacchi, R., 2003. Qualitative analysis of grapevine tannins by mass spectrometry and their inhibitory effect on stilbene oxidase of *Botrytis cinerea*. CHIMIA 57. https://doi.org/10.2533/000942903777678795, 607–607.

Pettenuzzo, S., Cappellin, L., Grando, M.S., Costantini, L., 2022. Phenotyping methods to assess heat stress resilience in grapevine. J. Exp. Bot. 73, 5128–5148. https://doi.org/10.1093/jxb/erac058.

Pezet, R., Perret, C., Jean-Denis, J.B., Tabacchi, R., Gindro, K., Viret, O., 2003a. δ-Viniferin, a resveratrol dehydrodimer: one of the major stilbenes synthesized by stressed grapevine leaves. J. Agric. Food Chem. 51, 5488–5492. https://doi.org/10.1021/jf030227o.

Pezet, R., Pont, V., Hoang-Van, K., 1991. Evidence for oxidative detoxication of pterostilbene and resveratrol by a laccase-like stilbene oxidase produced by *Botrytis cinerea*. Physiol. Mol. Plant Pathol. 39, 441–450. https://doi.org/10.1016/0885-5765(91)90010-F.

Pezet, R., Viret, O., Perret, C., Tabacchi, R., 2003b. Latency of *Botrytis cinerea* Pers.: Fr. and biochemical studies during growth and ripening of two grape berry cultivars, respectively susceptible and resistant to grey mould. J. Phytopathol. 151, 208–214. https://doi.org/10.1046/j.1439-0434.2003.00707.x.

Porter, W.L., Schwartz, J.H., 1962. Isolation and description of the pectinase-inhibiting tannins of grape leaves. J. Food Sci. 27, 416–418. https://doi.org/10.1111/j.1365-2621.1962.tb00119.x.

R Core Team, 2024. R: a Language and Environment For Statistical Computing. R Foundation for Statistical Computing.

Radler, F., 1965. The main constituents of the surface waxes of varieties and species of the genus *VITIS*. Am. J. Enol. Vitic. 16, 159–167. https://doi.org/10.5344/ajev.1965.16.3.159.

Rahman, M.U., Liu, X., Wang, X., Fan, B., 2024. Grapevine gray mold disease: infection, defense and management. Hortic. Res. 11, uhae182. https://doi.org/10.1093/hr/uhae182.

Rogiers, S.Y., Whitelaw-Weckert, M., Radovanonic-Tesic, M., Greer, L.A., White, R.G., Steel, C.C., 2005. Effects of spray adjuvants on grape (*Vitis vinifera*) berry microflora, epicuticular wax and susceptibility to infection by *Botrytis cinerea*. Australas. Plant Pathol. 34, 221–228. https://doi.org/10.1071/AP05031.

RStudio Team, 2024. RStudio: integrated development environment for R.

Salinas, J., Warnaar, F., Verhoeff, K., 1986. Production of cutin hydrolyzing enzymes by *Botrytis cinerea in vitro*. J. Phytopathol. 116, 299–307. https://doi.org/10.1111/j.1439-0434.1986.tb00924.x.

Sbaghi, M., Jeandet, P., Bessis, R., Leroux, P., 1996. Degradation of stilbene-type phytoalexins in relation to the pathogenicity of *Botrytis cinerea* to grapevines. Plant Pathol. 45, 139–144. https://doi.org/10.1046/j.1365-3059.1996.d01-101.x.

Scalbert, A., 1991. Antimicrobial properties of tannins. Phytochemistry 30, 3875–3883. https://doi.org/10.1016/0031-9422(91)83426-L.

Schirra, M., D'hallewin, G., Ben-Yehoshua, S., Fallik, E., 2000. Host–pathogen interactions modulated by heat treatment. Postharvest Biol. Technol. 21, 71–85. https://doi.org/10.1016/S0925-5214(00)00166-6.

Schneider, C.A., Rasband, W.S., Eliceiri, K.W., 2012. NIH image to ImageJ: 25 years of image analysis. Nat. Methods 9, 671–675. https://doi.org/10.1038/nmeth.2089.

Scholthof, K.-B.G., 2007. The disease triangle: pathogens, the environment and society. Nat. Rev. Microbiol. 5, 152–156. https://doi.org/10.1038/nrmicro1596.

Shain, L., Miller, J.B., 1982. Pinocembrin: an antifungal compound secreted by leaf glands of eastern cottonwood. Phytopathology 72, 877. https://doi.org/10.1094/Phyto-72-877.

Shelake, R.M., Wagh, S.G., Patil, A.M., Červený, J., Waghunde, R.R., Kim, J.-Y., 2024. Heat stress and plant–biotic interactions: advances and perspectives. Plants 13, 2022. https://doi.org/10.3390/plants13152022.

Shiraishi, M., 1993. Three descriptors for sugars to evaluate grape germplasm. Euphytica 71, 99–106. https://doi.org/10.1007/BF00023472.

Silva-Moreno, E., Brito-Echeverría, J., López, M., Ríos, J., Balic, I., Campos-Vargas, R., Polanco, R., 2016. Effect of cuticular waxes compounds from table grapes on growth, germination and gene expression in *Botrytis cinerea*. World J. Microbiol. Biotechnol. 32, 74. https://doi.org/10.1007/s11274-016-2041-4.

Simko, I., Piepho, H.-P., 2012. The area under the disease progress stairs: calculation, advantage, and application. Phytopathology 102, 381–389. https://doi.org/10.1094/PHYTO-07-11-0216.

Slowikowski, K., Schep, A., Hughes, S., Dang, T.K., Lukauskas, S., Irisson, J.-O., Kamvar, Z.N., Ryan, T., Christophe, D., Hiroaki, Y., Gramme, P., Abdol, A.M., Barrett, M., Cannoodt, R., Krassowski, M., Chirico, M., Aphalo, P., Barton, F., 2024. ggrepel: automatically position non-overlapping text labels with "ggplot2.".

Sternad Lemut, M., Sivilotti, P., Franceschi, P., Wehrens, R., Vrhovsek, U., 2013. Use of metabolic profiling to study grape skin polyphenol behavior as a result of canopy microclimate manipulation in a 'Pinot noir' vineyard. J. Agric. Food Chem. 61, 8976–8986. https://doi.org/10.1021/jf4030757.

Sweetman, C., Sadras, V.O., Hancock, R.D., Soole, K.L., Ford, C.M., 2014. Metabolic effects of elevated temperature on organic acid degradation in ripening *Vitis vinifera* fruit. J. Exp. Bot. 65, 5975–5988. https://doi.org/10.1093/jxb/eru343.

Tao, S., Zhang, S., Tsao, R., Charles, M.T., Yang, R., Khanizadeh, S., 2010. *In vitro* antifungal activity and mode of action of selected polyphenolic antioxidants on *Botrytis cinerea*. Arch. Phytopathol. Plant Prot. 43, 1564–1578. https://doi.org/10.1080/03235400802583834.

Tay, J.K., Narasimhan, B., Hastie, T., 2023. Elastic net regularization paths for all generalized linear models. J. Stat. Softw. 106, 1–31. https://doi.org/10.18637/jss.v106.i01.

Thomas, C.S., Marois, J.J., English, J.T., 1988. The effects of wind speed, temperature, and relative humidity on development of aerial mycelium and conidia of *Botrytis cinerea* on grape. Phytopathology 78, 260. https://doi.org/10.1094/Phyto-78-260.

Timperio, A.M., D'Alessandro, A., Fagioni, M., Magro, P., Zolla, L., 2012. Production of the phytoalexins *trans*-resveratrol and *delta*-viniferin in two economy-relevant grape cultivars upon infection with *Botrytis cinerea* in field conditions. Plant Physiol. Biochem. 50, 65–71. https://doi.org/10.1016/j.plaphy.2011.07.008.

Torres, N., Martínez-Lüscher, J., Porte, E., Yu, R., Kaan Kurtural, S., 2021. Impacts of leaf removal and shoot thinning on cumulative daily light intensity and thermal time and their cascading effects of grapevine (*Vitis vinifera* L.) berry and wine chemistry in warm climates. Food Chem. 343, 128447. https://doi.org/10.1016/j.foodchem.2020.128447.

Tsugawa, H., Cajka, T., Kind, T., Ma, Y., Higgins, B., Ikeda, K., Kanazawa, M., VanderGheynst, J., Fiehn, O., Arita, M., 2015. MS-DIAL: data-independent MS/MS deconvolution for comprehensive metabolome analysis. Nat. Methods 12, 523–526. https://doi.org/10.1038/nmeth.3393.

van Baarlen, P., Legendre, L., van Kan, J.A.L., 2007. Plant defence compounds against Botrytis infection. In: Elad, Y., Williamson, B., Tudzynski, P., Delen, N. (Eds.), Botrytis: Biology, Pathology and Control. Springer Netherlands, Dordrecht, pp. 143–161. https://doi.org/10.1007/978-1-4020-2626-3_9.

van Kan, J.a.L., van 't Klooster, J.W., Wagemakers, C.a.M., Dees, D.C.T., van der Vlugt-Bergmans, C.J.B., 1997. Cutinase A of *Botrytis cinerea* is expressed, but not essential, during penetration of gerbera and tomato. MPMI 10, 30–38. https://doi.org/10.1094/MPMI.1997.10.1.30.

van Leeuwen, C., Destrac-Irvine, A., Dubernet, M., Duchêne, E., Gowdy, M., Marguerit, E., Pieri, P., Parker, A., de Rességuier, L., Ollat, N., 2019. An update on the impact of climate change in viticulture and potential adaptations. Agronomy 9, 514. https://doi.org/10.3390/agronomy9090514.

van Schie, C.C.N., Takken, F.L.W., 2014. Susceptibility Genes 101: how to be a good host. Annu. Rev. Phytopathol. 52, 551–581. https://doi.org/10.1146/annurev-phyto-102313-045854.

VanderWeide, J., Yan, Y., Zandberg, W.F., Castellarin, S.D., 2022. Modulation of grape cuticular wax composition following multiple heatwaves influences grape transpiration. Environ. Exp. Bot. 202, 105036. https://doi.org/10.1016/j.envexpbot.2022.105036.

Venios, X., Korkas, E., Nisiotou, A., Banilas, G., 2020. Grapevine responses to heat stress and global warming. Plants 9, 1754. https://doi.org/10.3390/plants9121754.

Vignault, A., Gombau, J., Jourdes, M., Moine, V., Canals, J.M., Fermaud, M., Roudet, J., Zamora, F., Teissedre, P.-L., 2020. Oenological tannins to prevent *Botrytis cinerea* damage in grapes and musts: kinetics and electrophoresis characterization of laccase. Food Chem. 316, 126334. https://doi.org/10.1016/j.foodchem.2020.126334.

Vignault, A., Pascual, O., Jourdes, M., Moine, V., Fermaud, M., Roudet, J., Canals, J.M., Teissedre, P.-L., Zamora, F., 2019. Impact of enological tannins on laccase activity: special macrowine. OENO One 53. https://doi.org/10.20870/oeno-one.2019.53.1.2361.

Viret, O., Keller, M., Jaudzems, V.G., Cole, F.M., 2004. *Botrytis cinerea* infection of grape flowers: light and electron microscopical studies of infection sites. Phytopathology 94, 850–857. https://doi.org/10.1094/PHYTO.2004.94.8.850.

Viret, O., Spring, J.-L., Gindro, K., 2018. Stilbenes: biomarkers of grapevine resistance to fungal diseases. OENO One 52, 235–241. https://doi.org/10.20870/oeno-one.2018.52.3.2033.

Wang, H., Liu, M., Zhang, W., Yan, J., Tang, X., Sanchez-Molina, J.A., Li, X., 2023. An effect and less spraying control method successfully controls *Botrytis cinerea* on grapes in China. Agronomy 13, 2578. https://doi.org/10.3390/agronomy13102578.

Watrelot, A.A., Norton, E.L., 2020. Chemistry and reactivity of tannins in *Vitis* spp.: a review. Molecules 25, 2110. https://doi.org/10.3390/molecules25092110.

Weiller, F., Schückel, J., Willats, W.G.T., Driouich, A., Vivier, M.A., Moore, J.P., 2021. Tracking cell wall changes in wine and table grapes undergoing *Botrytis cinerea* infection using glycan microarrays. Ann. Bot. 128, 527–543. https://doi.org/10.1093/aob/mcab086.

Wickham, H., 2023. Stringr: simple, consistent wrappers for common string operations.

Wickham, H., 2020. reshape2: flexibly reshape data: a reboot of the reshape package.

Wickham, H., 2016. Data analysis. In: Wickham, H. (Ed.), Ggplot2: Elegant Graphics For Data Analysis. Use R! Springer International Publishing, Cham, pp. 189–201. https://doi.org/10.1007/978-3-319-24277-4_9.

Wickham, H., 2007. Reshaping data with the reshape package. J. Stat. Softw. 21, 1–20. https://doi.org/10.18637/jss.v021.i12.

Wickham, H., Chang, W., Henry, L., Pedersen, T.L., Takahashi, K., Wilke, C., Woo, K., Yutani, H., Dunnington, D., Brand, T. van den, Posit, PBC, 2024a. ggplot2: create elegant data visualisations using the grammar of graphics.

Wickham, H., François, R., Henry, L., Müller, K., Vaughan, D., 2023. dplyr: a grammar of data manipulation.

Wickham, H., Vaughan, D., Girlich, M., Ushey, K., 2024b tidyr: tidy messy data.

Wu, J., Abudureheman, R., Zhong, H., Yadav, V., Zhang, C., Ma, Y., Liu, X., Zhang, F., Zha, Q., Wang, X., 2023. The impact of high temperatures in the field on leaf tissue structure in different grape cultivars. Horticulturae 9, 731. https://doi.org/10.3390/horticulturae9070731.

Würz, D.A., Rufato, L., Bogo, A., Allebrandt, R., Pereira de Bem, B., Marcon Filho, J.L., Brighenti, A.F., Bonin, B.F., 2020. Effects of leaf removal on grape cluster architecture and control of Botrytis bunch rot in Sauvignon Blanc grapevines in Southern Brazil. Crop Prot. 131, 105079. https://doi.org/10.1016/j.cropro.2020.105079.

Xu, D., Deng, Y., Han, T., Jiang, L., Xi, P., Wang, Q., Jiang, Z., Gao, L., 2018. *In vitro* and *in vivo* effectiveness of phenolic compounds for the control of postharvest gray mold of table grapes. Postharvest Biol. Technol. 139, 106–114. https://doi.org/10.1016/j.postharvbio.2017.08.019.

Xu, H., Liu, Guojie, Liu, Guotian, Yan, B., Duan, W., Wang, L., Li, S., 2014. Comparison of investigation methods of heat injury in grapevine (*Vitis*) and assessment to heat tolerance in different cultivars and species. BMC Plant Biol. 14, 156. https://doi.org/10.1186/1471-2229-14-156.

Zhang, M., Zhang, P., Lu, S., Ou-yang, Q., Zhu-ge, Y., Tian, R., Jia, H., Fang, J., 2021. Comparative analysis of cuticular wax in various grape cultivars during berry development and after storage. Front. Nutr. 8, 817796. https://doi.org/10.3389/fnut.2021.817796.

Ziv, C., Zhao, Z., Gao, Y.G., Xia, Y., 2018. Multifunctional roles of plant cuticle during plant-pathogen interactions. Front. Plant Sci. 9, 1088. https://doi.org/10.3389/fpls.2018.01088.